iScience

Article

Single-cell transcriptomics reveals the multidimensional dynamic heterogeneity from primary to metastatic gastric cancer

Graphical abstract

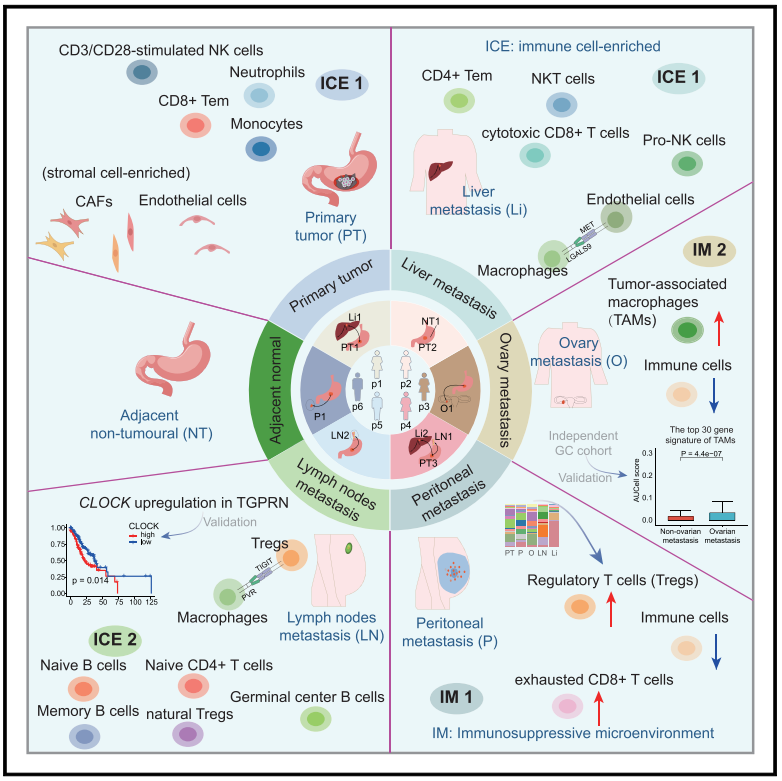

Highlights

- Immunosuppression in the tumor microenvironment of O and P
- A 30-gene signature of ovarian-derived TAMs was validated to predict O
- Dynamic changes in immune and stromal cell states during the PT-to-M progression
- Identification of new transcription factor CLOCK in the TGPRNs of metastatic GC

Authors

Yunpeng Zhang, Kuan Yang, Jing Bai, ..., Wenzhe Zhou, Xia Li, Congxue Hu

Correspondence

zhangyp@hrbmu.edu.cn (Y.Z.),
lixia@hrbmu.edu.cn (X.L.),
hucx1996@hrbmu.edu.cn (C.H.)

In brief

Biological sciences; Cancer; Transcriptomics

Zhang et al., 2025, iScience *28*, 111843
February 21, 2025
https://doi.org/10.1016/j.isci.2025.111843

CellPress

iScience

CellPress
OPEN ACCESS

Article

Single-cell transcriptomics reveals the multidimensional dynamic heterogeneity from primary to metastatic gastric cancer

Yunpeng Zhang,[1,2,3,*] Kuan Yang,[1] Jing Bai,[1] Jing Chen,[1] Qi Ou,[1] Wenzhe Zhou,[1] Xia Li,[1,*] and Congxue Hu[1,*]
[1]College of Bioinformatics Science and Technology, Harbin Medical University, Harbin 150081, Heilongjiang, China
[2]These authors contributed equally
[3]Lead contact
*Correspondence: zhangyp@hrbmu.edu.cn (Y.Z.), lixia@hrbmu.edu.cn (X.L.), hucx1996@hrbmu.edu.cn (C.H.)
https://doi.org/10.1016/j.isci.2025.111843

SUMMARY

Reprogramming of the tumor microenvironment (TME) plays a critical role in gastric cancer (GC) progression and metastasis. However, the multidimensional features between primary tumors and organ-specific metastases remain poorly understood. In this study, we characterized the dynamic heterogeneity of GC from primary to metastatic stages. We identified seven major cell types and 27 immune and stromal subsets. Immune cells decreased, while immunosuppressive cells increased in ovarian and peritoneal metastases. A 30-gene signature for ovarian metastasis was validated in GC cohorts. Additionally, critical ligand-receptor interactions, including *LGALS9-MET* in liver metastasis and *PVR-TIGIT* in lymph node metastasis, were identified as potential therapeutic targets. Furthermore, *CLOCK*, a transcription factor, was associated with poor prognosis and influenced immune cell interactions and migration. Collectively, this study provides valuable insights into TME dynamics in GC and highlights potential avenues for targeted therapies.

INTRODUCTION

Gastric cancer (GC) is a major global malignancy, ranking fifth in cancer incidence and fourth in cancer-related deaths, with particularly high prevalence in Asia, Eastern Europe, and Central America, where incidence rates are notably elevated.[1] Despite the implementation of surgical interventions, the prognosis of GC remains poor, with an overall five-year survival rate of less than 30%, primarily due to late-stage diagnoses and challenges associated with organ-specific metastasis.[2]

Metastasis is a major contributor to the poor prognosis of GC, yet the molecular mechanisms underlying this cellular behavior remain largely elusive.[3] Tumor cells possess the ability to invade distant sites via various routes, including blood circulation, the lymphatic system, direct infiltration, and transcoelomic spread.[4] During this metastatic process, tumor cells undergo adaptive changes, activating specific genes and pathways that enable them to thrive in particular organs. The interactions between the primary tumor, the host microenvironment, and immune cells recruited by the tumor play a pivotal role in driving metastatic progression.[5] To develop targeted therapeutic strategies and identify potential biomarkers for clinical diagnosis, it is crucial to accurately delineate the organ-specific features of metastasis. However, the current understanding of organ-specific metastasis in GC remains incomplete.

The exploration of GC diversity has advanced significantly with the application of single-cell transcriptome sequencing, a cutting-edge methodology.[6] While the conventional approach to investigating organ-specific metastasis typically involves transcriptome profiling, some researchers have employed bulk RNA sequencing (RNA-seq) to identify genes critical to site-specific metastases. The expression of these genes in the primary tumor has been linked to the recurrence of GC metastasis.[7] However, bulk methods have inherent limitations, particularly in discerning cell diversity, resulting in an oversight of the intricate intra- and inter-tumor complexity in GC.[8] The emergence of single-cell RNA sequencing (scRNA-seq) technology has revolutionized this landscape, enabling precise and comprehensive examination of intra- and inter-tumor heterogeneity across diverse cancer types.[9]

Transcription factors (TFs) play a crucial role in regulating gene expression and thereby exert indirect control over various cellular processes and states. Overexpression of specific TFs has the potential to induce significant alterations in cell fate, making them a promising approach to cancer diagnosis, prognosis, and treatment.[10] Therefore, to enhance our understanding of GC and develop potential therapeutic interventions, it is essential to identify cell-specific TFs in both primary and metastatic GC.

In this study, we characterized a total of 42,968 high-quality cells from six patients across 10 samples to identify seven major cell types and 27 unique immune and stromal cell subsets within the TME of primary and metastatic GC. Our analysis comprehensively explored cellular compositions, developmental trajectories, cell interactions, and transcriptional regulation between primary tumors and metastases. These findings provide valuable

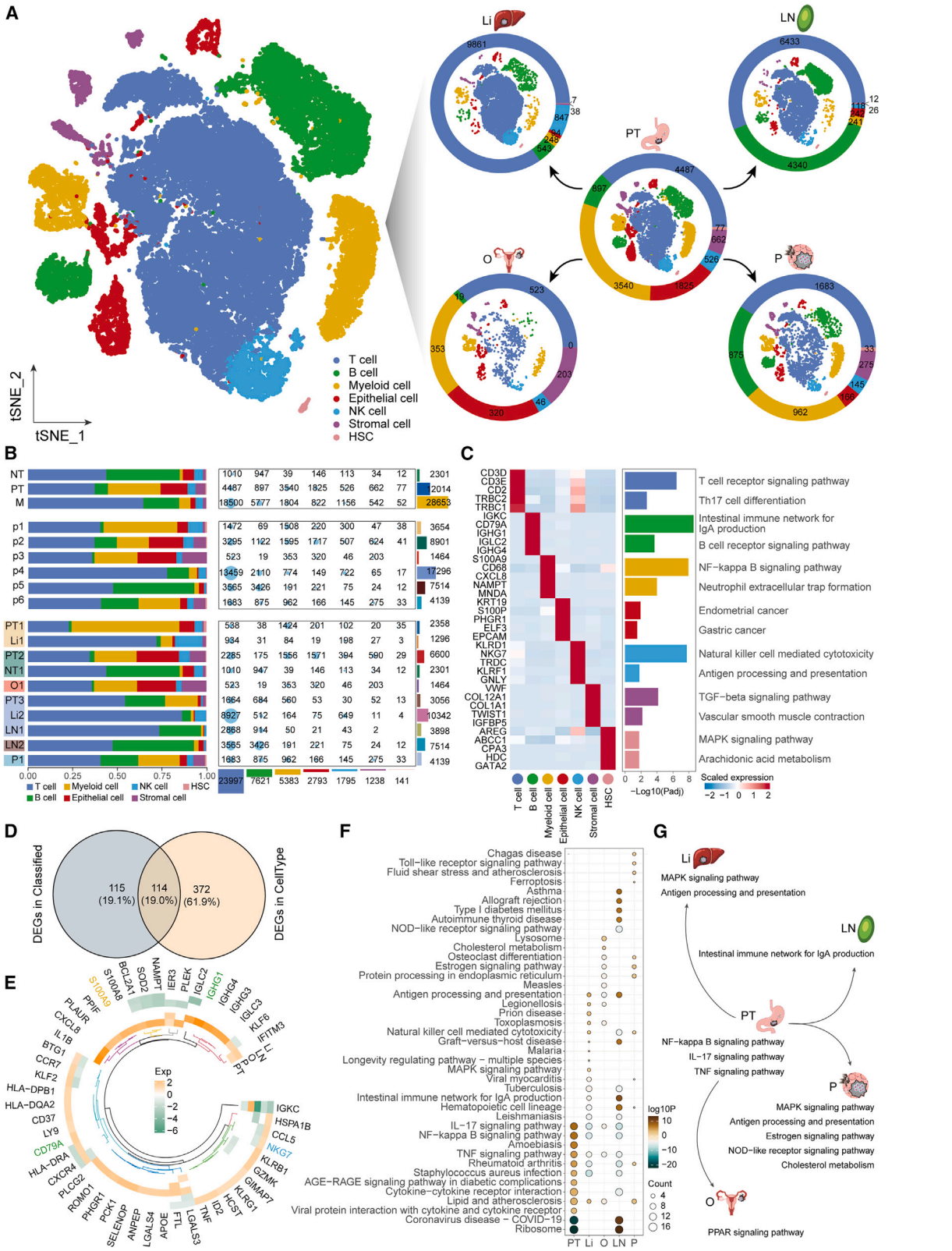

(legend on next page)

insights into the cellular, molecular, and functional changes during GC progression. Furthermore, we constructed a cell-specific TFs regulatory network in both primary and metastatic GC, enhancing our understanding of the transcriptional mechanisms driving the progression from primary to metastatic GC. Our study paves the way for future investigations and offers a valuable resource for subsequent academic research.

RESULTS

Remodeling the single-cell transcriptional landscape reveals insights into primary-to-metastatic GC progression

We performed an in-depth analysis of single-cell transcriptomic data obtained from the Gene Expression Omnibus (GEO) dataset GSE163558,[8] which comprises 10 human tissue samples from six patients. Our sample cohort included three primary tumor samples (PT1, PT2, and PT3), one adjacent non-tumor sample (NT1), and six unique metastatic samples (M): liver metastasis (Li1 and Li2), lymph node metastasis (LN1 and LN2), peritoneal metastasis (P1), and ovarian metastasis (O1). Specifically, PT1 and Li1 were from patient 1 (p1); PT2 and NT1 were from patient 2 (p2); O1 was from patient 3 (p3); PT3, Li2, and LN1 were from patient 4 (p4); LN2 was from patient 5 (p5); and P1 was from patient 6 (p6). After rigorous quality control, 42,968 cells were retained for subsequent analysis, with an average of 1,639 genes, 5,529 unique molecular identifiers (UMIs), and only about 6% mitochondrial genes per cell detected (Figures S1B–S1D). Interestingly, the proportion of ribosomal genes, as well as their correlation with nCount_RNA and nFeature_RNA, was found to be very low. Unsupervised clustering, based on transcriptome similarity, identified 12 distinct cell clusters, which were visualized using the t-distributed stochastic neighbor embedding (tSNE) analysis. The spatial distribution of cells from each patient and sample was also obtained (Figure S1A). Correlation analysis validated the reliability of the clusters, demonstrating that clusters from the same cell lineage exhibited higher similarity than those from different lineages (Figure S1E).

Immune cells accounted for the majority of our analyzed cells from the GC samples, particularly in the lymph node and liver, which has also been observed in other scRNA-seq studies of cancer.[11] We identified seven major cell types using the following markers: T cells (e.g., *CD3D*, *CD3E*, *CD2*), B cells (e.g., *CD79A*, *IGHG1*, *IGHG3*), myeloid cells (e.g., *CD68*, *CXCL8*), natural killer (NK) cells (e.g., *KLRD1*, *GNLY*, *KLRF1*), epithelial cells (e.g., *EPCAM*, *KRT19*, *ELF3*), stromal cells (e.g., *VWF*, *COL1A1*, *COL12A1*), and hematopoietic stem cells (HSCs) (e.g., *AREG*, *ABCC1*, *GATA2*). Intriguingly, gene ontology (GO) analysis showed that multiple mast cell-associated pathways were enriched in HSCs (Figure S1G), indicating that HSCs have the potential to differentiate into mast cells under certain conditions, may be involved in mast cell-related immune responses or tumor progression. These cell clusters were characterized by marker gene expression and distinct physiological functions, exhibited distinct distributions during GC primary to metastatic (PT-to-M) progression (Figures 1A–1C and S1F and Table S1). Notably, myeloid, epithelial, and stromal cells showed decreasing trends during PT-to-M progression, whereas B cells exhibited an increasing trend during GC lymph node metastasis progression, and T cells showed an increasing trend during both GC lymph node and liver metastasis progression (Figures 1A and 1B).

Next, we explored the dynamic changes in the TME from additional perspectives. At the molecular level, we identified 114 overlapping genes as potential markers during PT-to-M progression, revealing a correlation between changes in the cellular compositions and the expression of cellular marker genes (Figure 1D). *CD79A*, a marker gene of B cells, was specifically expressed in LN, suggesting a link between its expression and the increasing trend of B cells in LN (Figure 1E). Additionally, we performed Kyoto Encyclopedia of Genes and Genomes (KEGG) enrichment analysis on the differentially expressed genes (DEGs) in our cancer samples, which provided insights into the functional differences between PT and M (Figure 1F and Table S2). The activation of the NF-κB signaling, IL-17 signaling, and TNF signaling pathways in PT suggested dynamic interactions between cancer cells and the immune and inflammatory components of the TME.[12] Furthermore, Li exhibited enrichment for the MAPK signaling pathway, and O showed specific enrichment for cholesterol metabolism. We also observed the activation of ferroptosis in P, a phenomenon reported in other studies,[13] indicating the involvement of cell death regulation in GC peritoneal metastasis.[14] Together, the KEGG pathway enrichment analysis indicated that cells undergo significant functional reprogramming during PT-to-M progression, with upregulated antigen processing and presentation pathways observed during the progression of GC liver and peritoneal metastasis (Figures 1G and S1H).

Immunosuppression in the TME of GC ovarian and peritoneal metastasis and a 30 gene signature of ovarian-derived TAMs was validated to predict ovarian metastasis

Sub-clustering analyses of immune and stromal cells identified 27 cell subsets (Figures 2A and S2A). T cells were divided into nine clusters: $CD8^+$ T cells, naive $CD8^+$ T cells, naive $CD4^+$

Figure 1. Single-cell atlas of primary tumor, metastasis, and adjacent non-tumor samples

(A) tSNE visualization highlighting seven distinct cell types among the 42,968 cells (left), delineating the TME cell clusters across different tissue groups (right).

(B) Proportion of each cell type in various samples (NT, PT, M, Li, LN, P, and O) and patients (p1-p6).

(C) Left: heatmap showing the expression profiles of the top five genes ranked by LogFC of each cell type. Right: enriched KEGG pathways for the marker genes of each cell type.

(D) Venn diagram for the overlap analysis of the marker genes across the seven cell types and five cancer samples.

(E) Ring heatmap visualizing the marker genes specific to each of five cancer samples.

(F) Dot plot showing the enrichment pathways in the five cancer samples based on the DEGs using KEGG enrichment analysis.

(G) Functional changes during PT-to-M progression.

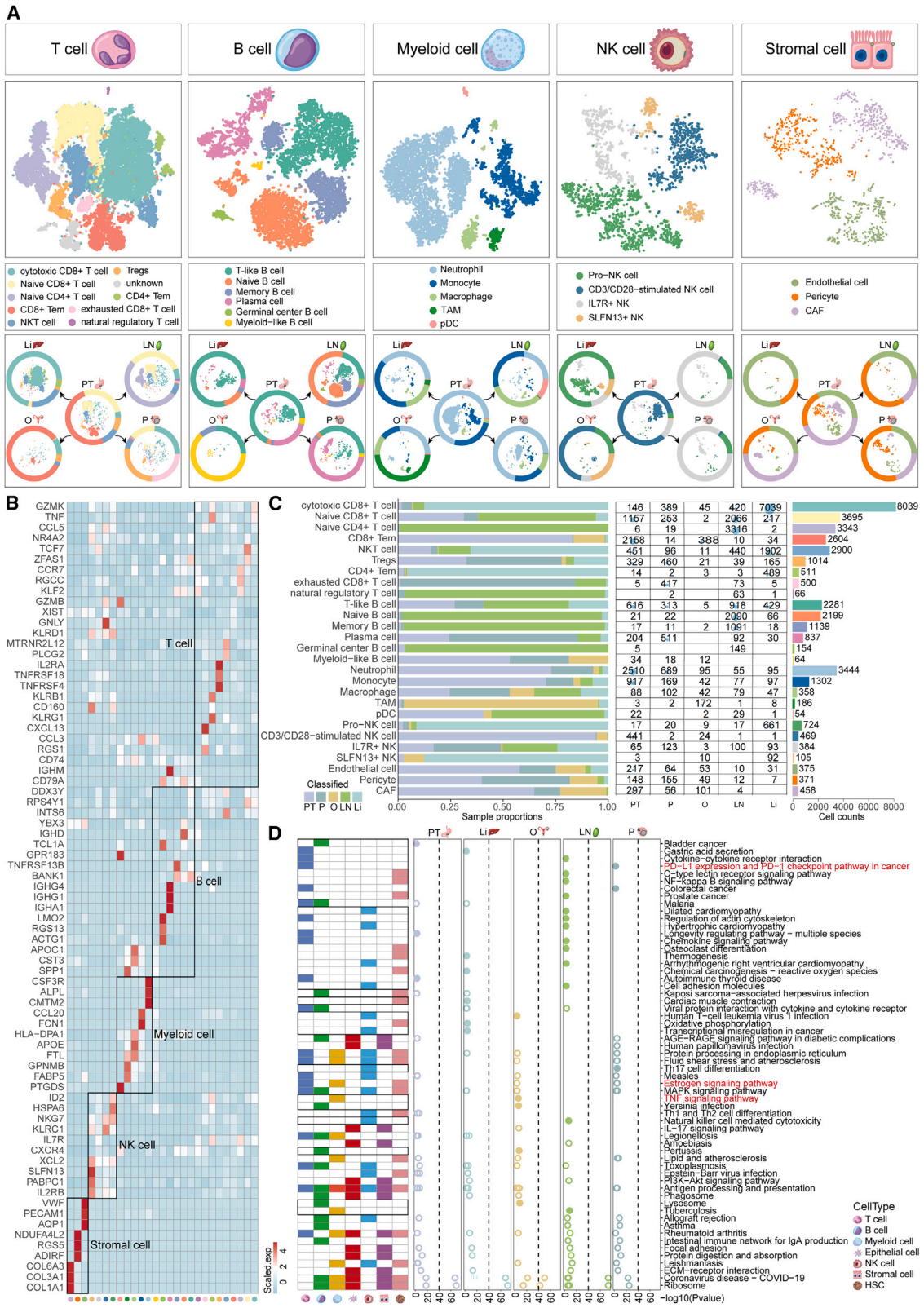

(legend on next page)

T cells, $CD8^+$ T effector memory (Tem) cells, natural killer T (NKT) cells, regulatory T cells (Tregs), $CD4^+$ T effector memory (Tem) cells, exhausted $CD8^+$ T cells, and natural regulatory T cells. B cells were primarily composed of six subgroups: T cell-like B cells,[8] naive B cells, memory B cells, plasma cells, germinal center (GC) B cells, and myeloid-like B cells (M-B cells). Myeloid cells were further divided into five subsets: neutrophils, monocytes, macrophages, tumor-associated macrophages (TAMs), and plasmacytoid dendritic cells (pDCs). NK cells were subdivided into four subclusters: NK cell progenitors (Pro-NK cells), CD3/CD28-stimulated NK cells, IL7R + NK cells, and SLFN13+ NK cells. Stromal cells were categorized into endothelial cells, pericytes, and cancer-associated fibroblasts (CAFs). Notably, each cluster exhibited a distinct gene expression pattern (Figure 2B and Table S3). Correlation analysis revealed that clusters from the same cell lineage showed higher similarity to one another than to those from other lineages (Figure S2B), confirming the reliability of the clustering. The distribution of UMIs in each cell lineage is shown in Figure S2C. These results highlight a high degree of cell state diversity within the TME of primary and metastatic GC.

These cell clusters exhibited distinct distributions during GC progression (Figures 2C and S2D). Specifically, $CD8^+$ Tem cells, neutrophils, monocytes, CD3/CD28-stimulated NK cells, endothelial cells, and CAFs subsets showed a decreasing trend during the PT-to-M progression. In contrast, cytotoxic $CD8^+$ T cells, NKT cells, $CD4^+$ Tem cells, Pro-NK cells, and SLFN13+ NK cells exhibited an increasing trend during GC liver metastasis progression. Notably, in addition to Tregs and exhausted $CD8^+$ T cells, several other TME cell subsets, including macrophage subsets, CAFs, endothelial cells, and pericytes, exhibited high expression of inhibitory immune checkpoint receptors (Figure S4A), well-known immunosuppressive molecules, and cytokines such as IL-10, suggesting their immunosuppressive phenotypes.[13] Additionally, TAMs exhibited the highest expression of *SPP1*, an angiogenesis-related gene, along with *SIRPA* and the M2-like signature.[15,16] Intriguingly, we observed that TAMs showed increasing trends in O, while Tregs and exhausted $CD8^+$ T cell showed increasing trends in P, indicating the establishment of an immunosuppressive microenvironment. Furthermore, naive $CD8^+$ T cells, naive $CD4^+$ T cells, naive B cells, memory B cells, and GC B cells exhibited increasing trends during GC lymph node progression, indicating an active immune response. Importantly, GC B cells were exclusively expressed in the lymph node, demonstrating a characteristic of "metastatic expression." Together, these findings indicate that both exhausted $CD8^+$ T cells and cytotoxic $CD8^+$ T cells exhibited increasing trends during PT-to-M progression, highlighting that T cell exhaustion leads to diminished effector function, preventing cytotoxic $CD8^+$ T cells from controlling tumor progression.

When focusing on the expression of specific genes across the cell clusters between PT and M, a shared gene set across seven distinct cellular microenvironments revealed a correlation between cellular compositions and the expression of marker genes (Figures S3A and S3B). KEGG analysis was conducted to explore the potential biological functions and relevant signaling pathways in each cell type for each cancer sample (Figures 2D and S5A–S5E, Tables S4 and S5). Myeloid cell subsets in O were enriched in the TNF signaling pathway, indicating that a reduction in myeloid cell populations contributes to immune suppression during GC ovarian metastasis through activation of the TNF pathway.[17] A recent study has shown that immune-checkpoint molecules are involved in tumor immune evasion.[18] Meanwhile, we found that multiple metabolism pathways were positively regulated in TMAs (Figure S5C), indicating that TAMs may promote GC ovarian metastasis via metabolic reprogramming.[19] PD-L1 expression and the PD-1 checkpoint pathway were activated in T cell subsets in P, suggesting immune suppression mediated by the PD-1/PD-L1 axis.[17] Next, many pathways closely related to inflammatory response were observed in Tregs, such as cytokine-cytokine receptor interaction pathway and NF-κB signaling pathway, whereas pathways associated with immune diseases were enriched in exhausted $CD8^+$ T cells (Figure S5A). More interestingly, the estrogen signaling pathway was activated in both ovarian and peritoneal metastases, potentially regulating the growth of GC cells in an immunosuppressive state.[20]

Ovarian metastasis of gastric cancer signifies an advanced stage of the disease, where opportunities for radical surgery become limited.[21] Thus, identifying the signature of ovarian metastasis at single-cell resolution holds significant clinical value. We performed a differential expression analysis of single-cell DEGs for each myeloid subpopulation between ovarian-derived and non-ovarian-derived subsets, focusing on the top 30 upregulated DEGs in the ovarian-derived subset. As shown in Figure S4B, TAMs in the ovarian-derived subset exhibited higher expression of these top 30 upregulated DEGs in O compared to other metastatic sites. In Figure S4C, the 30-gene signature of TAMs was validated using an independent GC cohort (GSE239676). Further analysis evaluated the prognostic significance of this 30-gene signature in TAMs derived from ovarian metastasis samples within a large-scale GC cohort (GSE84437). The results revealed that patients with high scores for this 30-gene signature in ovarian metastasis-derived TAMs had significantly shorter survival than those with lower scores ($p < 0.0001$) (Figure S4D), underscoring the potential of this 30-gene signature in predicting patient survival. These findings

Figure 2. Subclusters of immune and stromal cells characterized during GC progression

(A) tSNE showing 27 unique immune and stromal cell subsets (upper panels) and their corresponding TME cell clusters (lower panels) across different tissue groups.

(B) Heatmap of the expression of subset-specific markers across cell subsets.

(C) Reproducible cell subset distributions across the five cancer samples.

(D) Heatmap showing tissue preferences of clusters in each immune and stromal cell subsets revealed by Ro/e (ratio of observed cell number to expected cell number). Dot plot showing the bio functions of modules based on DEGs by GO.

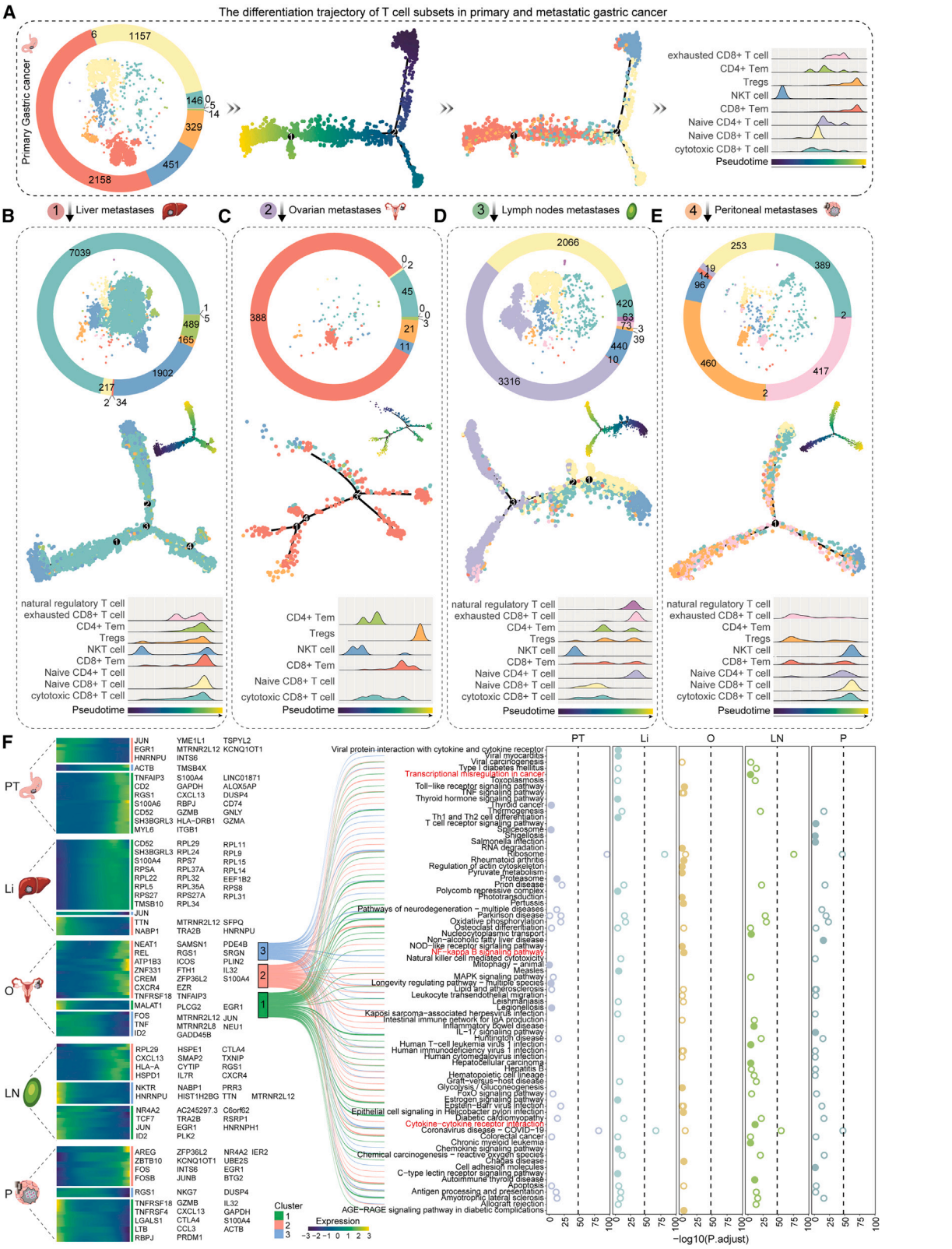

(legend on next page)

highlight the role of specific cellular compositions and functional pathway activations in immunosuppression, which may inform clinical strategies for treating GC patients.

Dynamic changes in immune and stromal cell states during GC primary-to-metastatic progression

Single-cell trajectories revealed the temporal evolution of diverse cell types, helping to define distinct cellular states in specific microenvironments. Using Monocle trajectory analysis to explore the developmental trajectories of immune and stromal cell subsets in both PT and M (see STAR Methods), we found that the developmental trajectory of the T cell subsets was specific to P. This path began with exhausted $CD8^+$ T cells, Tregs, and $CD8^+$ Tem cells, culminating in NKT cells (Figures 3A–3E), suggesting a distinct immunological response or microenvironmental influence specific to GC peritoneal metastasis. We further analyzed the expression changes of genes associated with cell transitions. In the origin of the developmental trajectory of T cell subsets in O, where NKT cells were enriched, the cells were characterized by NF-κB, a pivotal regulator of cancer metastasis and therapeutic response[22] (Figure 3F). The developmental trajectory of T cell subsets in LN started with NKT cells, which were linked to transcriptional mis-regulation in cancer—a process that has been shown to contribute to the development and maintenance of the cancer phenotype.[23] At the end of this trajectory in LN, where naive $CD8^+$ T cells and natural regulatory T cells were enriched, the cells were characterized by cytokine-cytokine receptor interaction, which were known to regulate cell growth, differentiation, cell death, angiogenesis, and development.[24]

Unique cellular compositions may lead to a distinct developmental trajectory. We found that the B cell subsets in O followed a specific developmental trajectory (Figures S4A–S4E), starting with M-B cells and culminating in T cell-like B cells. The cells were characterized by upregulation of PPAR signaling, which is known to be linked to GC development and metastasis[25] (Figure S6F). At the end of the developmental trajectory of B cell subsets in LN, where T cell-like B cells were enriched, the cells were characterized by activation of MAPK signaling, which is known to promote GC progression.[26] In contrast, the B cell lineage trajectory in P revealed that plasma cells were at the origin of the development trajectory, and these cells were associated with epithelial-mesenchymal transition[27] and cell adhesion molecules, suggesting a program linked to plasticity, therapy resistance, tumor growth, and metastases.[28] In addition, we observed that TAMs in O were involved in specific pathways such as "transcriptional mis-regulation in cancer" and "epithelial cell signaling in helicobacter pylori infection" at the origin of the developmental trajectory, highlighting its crucial role in cancer development and metastasis[29] (Figures S7A–S7F). Intriguingly, NK cell subsets displayed an opposite developmental trajectory in LN and P (Figures S8A–S8E). In P, where Pro-NK cells were enriched, the cells were characterized by PI3K-Akt signaling, which influences autophagy, epithelial-mesenchymal transition (EMT), apoptosis, chemoresistance, and metastasis in GC[30] (Figure S8F). Conversely, at the end of the trajectory in LN, where SLFN13+ NK cells were enriched, the cells were linked to "proteoglycans in cancer" and "cell cycle" pathways, suggesting potential biomarkers for cell cycle regulator application in GC treatment.[31]

We next explored stromal phenotype changes along the developmental trajectory during PT-to-M progression. Intriguingly, we found that PT, O, and LN followed a similar trajectory, beginning with endothelial cells, passing through pericytes, and culminating in CAFs. In contrast, P and Li exhibited opposite trajectories (Figures S9A–S9E). At the origin of the trajectory in PT, where endothelial cells were enriched, the cells were characterized by upregulation of cell adhesion molecules (Figure S9F). Notably, at the middle and end of the trajectory in Li, where endothelial cells were enriched, the cells were associated with cytokine-cytokine receptor interaction and PPAR signaling. In addition, we found that pericytes were enriched at the middle of the trajectory in O, and these cells were associated with viral carcinogenesis. In LN, where pericytes were also enriched at the midpoint of the trajectory, cells were linked to Wnt signaling, suggesting a potential therapeutic strategy for targeting this pathway.[32] In P, we observed that endothelial cells were enriched at the end of the trajectory, and these cells were involved in cellular senescence and the TGF-beta signaling pathway. The activation of TGF-beta signaling is known to suppress the proliferation and invasiveness of GC cells, potentially contributing to therapeutic strategies for GC oncotherapy.[33] These findings reveal dynamic changes in immune and stromal cell subsets during PT-to-M progression, offering valuable insights into potential therapeutic strategies for treating GC.

Ligand-receptor mediated intercellular interactions in the primary and metastatic GC microenvironment

To further clarify cellular regulation during GC progression, we analyzed cell interactions across all cell clusters in the ecosystem of primary and metastatic GC using CellPhoneDB. Our analysis revealed complex communication between stromal

Figure 3. Dynamic characterization of immune and stromal cells

(A) Changes in the T cell subsets of PT. Left to right: tSNE view of eight T cell clusters, developmental trajectory plot of T cell subsets color-coded by pseudotime and cluster (each dot represents a single cell), and cell density plots of the T cell subsets along the pseudotime. Top to bottom: tSNE view of the T cell clusters, developmental trajectory plot of the T cell subsets color-coded by cluster and pseudotime (each dot represents a single cell), and cell density plots of the T cell subsets along the pseudotime.

(B) Changes in the T cell subsets of Li. Details are described previously.

(C) Changes in the T cell subsets of O. Details are described previously.

(D) Changes in the T cell subsets of LN. Details are described previously.

(E) Changes in the T cell subsets of P. Details are described previously.

(F) Heatmap showing the dynamic expression changes in genes in the T cell clusters of PT, Li, O, LN, and P (left panel). Dot plot showing the top 10 enriched pathways in the five cancer samples based on the expressed genes along the cell trajectory using KEGG enrichment analysis (right panel). Solid circles indicate state-specific enrichment in the single-cancer samples.

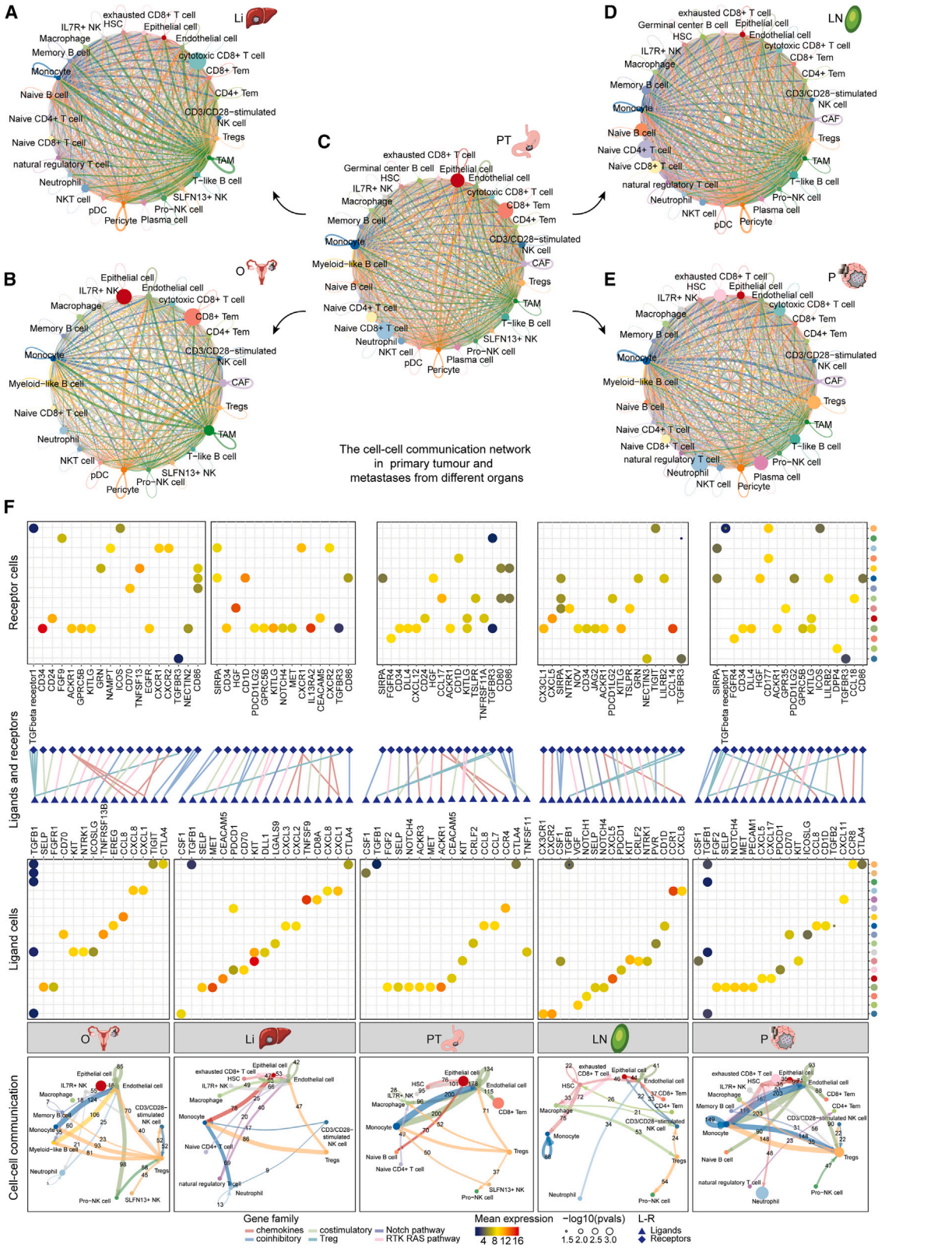

(legend on next page)

and other cells. Notably, the strongest cell interactions were observed between CAFs and endothelial cells in O, PT, and P (Figures 4B, 4C, 4E, S10B, S10C, and S10E), while CAFs exhibited the strongest interactions with pericytes in LN (Figures 4D and S10D). In Li, the strongest cell interactions occurred among monocytes, pericytes, and TAMs (Figures 4A and S10A).

We also identified several ligand-receptor interactions between clusters in PT and M, as shown in Figure 4F and Tables S6 and S7. These interactions revealed that different ligand-receptor pairs and cells play distinct roles in PT-to-M progression. For example, chemokine ligand-receptor pairs, including *ACKR3-CXCL12*, *ACKR1-CCL17*, *CCR4-CCL17*, *CCL7-ACKR1*, and *TNFSF11-TNFRSF11A* (Figures 4F and S11C) were specifically expressed in PT. Notably, naive $CD4^+$ T cells secreted *CCR4*, which binds to *CCL17* on macrophages. This interaction has been implicated in cancer cell metastasis and the activation of Tregs, thereby inhibiting antitumor immune responses.[34]

Additionally, interactions between PT and M showed clearly differences. For example, in Li, several ligand-receptor pairs, such as *TNFSF9-IL13RA2*, *DLL1-NOTCH4*, *LGALS9-MET*, *CD8A-CEACAM5*, *CXCL1-CXCR2*, and *CXCL3/CXCL2-CXCR1* were observed compared to PT (Figures 4F and S11A). Notably, IL7R + NK secreted *DLL1*, which binds to *NOTCH4* on endothelial cells, potentially disrupting tumor vascular integrity and promoting metastatic growth.[35] Moreover, macrophages secreted *LGALS9*, which binds to *MET* on endothelial cells. This interaction was associated with the RTK/RAS pathway and may serve as a potential marker for poor clinical outcomes.[36] In O, we observed a variety of ligand-receptor pairs, including *TNFRSF13B-TNFSF13*, *TNFRSF13B-CD70*, *TIGIT-NECTIN2*, *NTRK1-NAMPT*, *FGFR1-FGF9*, *EREG-EGFR*, and *CXCL1-ACKR1* (Figures 4F and S11B), which are also correlated with the RTK/RAS pathway.[37] Notably, Tregs secreted *TIGIT*, which binds to *ENCTIN2* on endothelial cells, potentially contributing to the immunosuppressive environment.[38] Monocytes secreted *EREG*, which binds to *EGFR* on endothelial cells, suggesting that targeting the *EREG-EGFR* axis could have therapeutic potential for inhibiting tumor progression.[39] In LN, specific ligand-receptor pairs, such as *VGF-NTRK1*, *NOTCH1-NOV*, *NOTCH4-JAG2*, *PVR-TIGIT*, *PVR-NECTIN3*, *CXCR2-CXCL5*, *CX3CR1-CX3CL1*, and *CCR1-CCL14*, were highly expressed (Figures 4F and S11D). Notably, macrophages secreted *PVR*, which binds to *TIGIT* on Tregs, making this interaction a potential target for immune checkpoint therapy.[40] CD3/CD28-stimulated NK cells secreted *CXCR2*, which binds to *CXCL5* on epithelial cells, potentially enhancing tumor metastasis.[41] In P, we identified specific ligand-receptor pairs such as *TGFB2*-TGFbeta receptor1, *CXCL17-GPR35*, *CXCL11-DPP4*, and *CCR8-CCL18* were expressed (Figures 4F and S11E). Epithelial cells secreted *CXCL17*, which binds to *GPR35* on HSCs, influencing tumor proliferation, migration, and invasion through the IL-17 pathway.[42] These results suggest that the TME differs significantly between PT and M, highlighting unique ligand-receptor interactions in each metastatic niche. This provides valuable insights for developing targeted therapies aimed at GC primary tumors and specific organ-associated metastases.

CLOCK favors the mutual attraction and migration of tumor and immune cells in lymph node metastasis and poor survival

TFs play crucial roles in regulating chromosome structure, gene transcription, and expression, with significant implications in tumorigenesis and cancer development.[43] To better understand the intricate regulatory landscape during tumor progression, we conducted a comprehensive analysis of the transcriptional regulatory mechanisms in the cellular microenvironments of both PT and M. Using pySCENIC analysis, we predicted 339 TFs across 28 cell types in PT and 329 TFs across 29 cell types in M (Figures S12A and S12B and Table S8). Notably, 129 TFs were identified in PT but were absent in M, suggesting that these TFs may have distinct regulatory roles specific to the tumor microenvironment of the primary site, which may not be recapitulated in metastatic tissues.

To assess the role of the predicted TFs in cancer development and metastasis, we conducted survival analysis using data from The Cancer Genome Atlas (TCGA) gastric adenocarcinoma cohort (TCGA-STAD.htseq_counts.tsv dataset, n = 407). This analysis focused on genes linked to cancer cells in both PT and M, revealing 17 TFs associated with survival prognosis in PT and 27 TFs in M (Figures S13A and S13B). Intriguingly, we observed that certain TFs, such as *RUNX2*, *ZNF143*, *SMAD5*, and *MEIS1*, were significantly negatively correlated with the survival of GC patients. Previous studies have suggested that *RUNX2* and *ZNF143* are involved in promoting malignant progression and metastasis in GC.[44] In M, we identified 14 TFs specifically expressed, including *KDM5B*, *ZNF101*, *SOX5*, *TCF7L1*, *GLIS3*, *NR1H4*, *CLOCK*, *TCF7*, *FOXD4L5*, *SOX7*, *HOXD3*, *ZNF471*, *ZNF571*, and *SP1*. Among of these TFs, *KDM5B*, *TCF7L1*, *TCF7*, *GLIS3*, *SOX7*, *ZNF471*, and *SP1* have previously been linked to GC development and prognosis.[45–51] To further validate our findings and uncover the transcriptional heterogeneity between primary GC and different organ-specific metastases, we integrated data on the DEGs and functional pathways from five cancer samples within each cellular microenvironment, leading to the identification of 21 key TFs (Figure S12C).

Figure 4. Complex intercellular communication networks in the TME of PT and M

(A) The intercellular communication networks from Li, demonstrating the strength of the interactions between all cell populations, with line thickness proportional to the strength of the interactions and line color consistent with the ligand cell type. The size of the dots represents the number of cells.

(B) The intercellular communication networks from O. Details are described previously.

(C) The intercellular communication networks from PT. Details are described previously.

(D) The intercellular communication networks from LN. Details are described previously.

(E) The intercellular communication networks from P. Details are described previously.

(F) Dot plots showing scaled z-scored expression of the genes coding for interacting ligand-receptor proteins (CellPhoneDB) in specific cell states from the TME of PT, Li, O, LN, and P. Specific interacting partners are linked with a matching symbol. Triangles represent ligands and diamonds represent receptors.

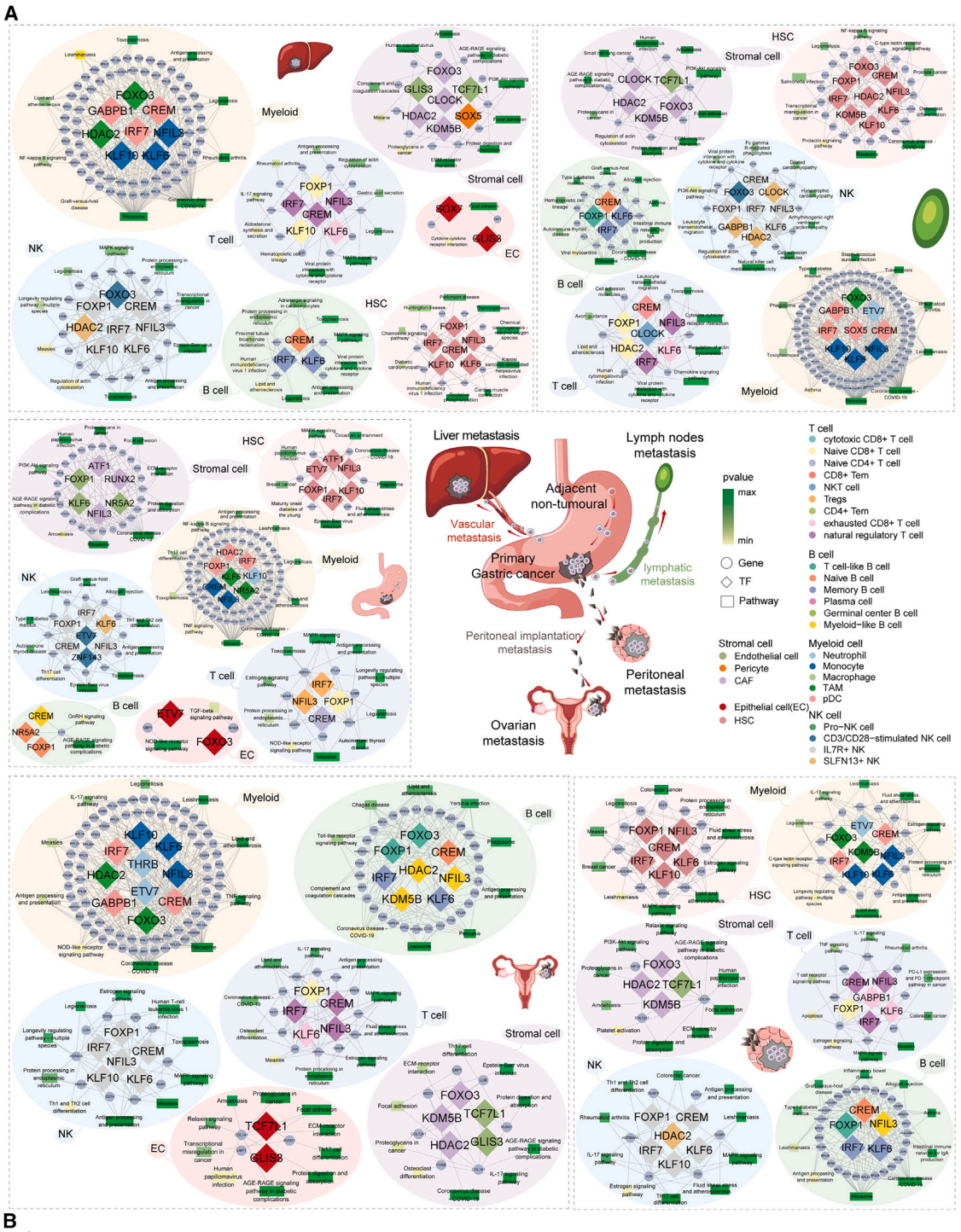

(legend on next page)

Transcriptional regulatory network analyses may provide valuable insights into gene regulation and the underlying mechanisms of dysfunction.[52] In our study, we constructed cell-specific TGPRNs for both primary and metastatic GC, aiming to explore the transcriptional heterogeneities. In the TGPRNs of PT (Figure 5A and Table S9), we observed high expression of CAFs-specific TF *RUNX2*. *RUNX2* was found to regulate its target gene *COL1A2*, which in turn activated the PI3K-Akt signaling pathway, strengthened cell-to-cell adhesion, and contributed to tumor cell metastasis.[53] Additionally, another TF, *ZNF143*, originating from CD3/CD28-stimulated NK cells, was associations with pathways such as Epstein-Barr virus infection and Th1 and Th2 cell differentiation. Notably, *ZNF143*, by regulating its target gene *RUNX3*, might influence immune cell differentiation and immune responses, particularly in the context of viral infections.[54]

In the TGPRNs of Li, we observed the specific expression of the TF *SOX7* from epithelial cells and *SOX5* from pericytes. These two TFs regulated the target genes LIFR and *COL14A1*, respectively. *SOX7* and *LIFR* were associated with cytokine-cytokine receptor interaction, while *SOX5* and *COL14A1* were linked to protein digestion and absorption,[55] suggesting their potential roles in protein breakdown and absorption during the progression of GC liver metastasis. In the TGPRNs of O, we observed that the TF *THRB* from neutrophils regulated the target gene *TNFSF10*, which was enriched in the lipid and atherosclerosis pathway. Additionally, the TF *KDM5B*, originating from M-B cells and specifically expressed in the TGPRNs of O, regulated the immune and inflammatory response through its target gene *CCL3* in the Toll-like receptor signaling pathway, suggesting a potential therapeutic target in GC ovarian metastasis.[56] In the TGPRNs of P, we observed that *GABPB1*, a TF from exhausted $CD8^+$ T cells, and its regulated target gene *BATF*, were associated with the PD-1 checkpoint pathway and PD-L1 expression in cancer.[57] This finding indicates that *GABPB1* and *BATF* might regulate the PD-1 and PD-L1 immune checkpoints during the progression of GC peritoneal metastasis, providing insights for developing immunotherapy strategies.[58] Notably, in the TGPRNs of LN, there was enrichment in the chemokine signaling pathway, regulated by the TF *CLOCK* from NKT cells. *CLOCK* and its target gene *CCL5* play roles in the attraction and migration of tumor and immune cells by regulating chemokine signaling.[59] Intriguingly, we found that, in addition to gastric cancer, *CLOCK* is also highly expressed in other cancers, including breast cancer (BRCA), liver hepatocellular carcinoma (LIHC), and prostate cancer (PRAD) (Figure S13C) (see STAR Methods). Notably, high *CLOCK* expression is associated with poor prognosis in BRCA (Figure S13D), suggesting its potential as a prognostic marker and therapeutic target in GC lymph nodes metastasis. The correlation between decreased expression of key TFs and improved survival prognosis revealed their critical regulatory roles in PT-to-M progression (Figure 5B). Our findings regarding cell-specific TGPRNs for both PT and M provide a theoretical framework for understanding the key TFs involved in GC progression and offer potential targets for innovative therapeutic approaches.

DISCUSSION

The complex intra- and inter-tumor heterogeneity in both primary and metastatic GC poses a great challenge to the efficacy of both chemotherapy and immunotherapy, limiting treatment outcomes and prognosis prediction.[60] Despite previous efforts to classify tumors using whole-sample transcriptomic approaches,[61] the heterogeneous nature of the TME introduces substantial limitations to the clinical applicability of such methods. The advent of scRNA-seq has provided insight into the TME.[62] In this study, we performed a detailed single cell analysis of primary and metastatic tumor sites, uncovering distinct and dynamic heterogeneity within the TME of GC.

To offer a high-resolution map of the molecular and cellular mechanisms of the malignant progression of GC, we performed a multidimensional analysis, including cellular compositions, developmental trajectories, cell interactions, and transcriptional regulation. Thus, our study provides a unique insight into the PT-to-M progression, compared to previous single-cell studies.[8,13,63] We present comprehensive single-cell landscape of primary and metastatic GC, revealing multiple immune cell clusters were enriched in liver metastasis and lymph node metastasis, which has previously been reported.[9,11,64] Moreover, we observed that TAMs were predominantly enriched in ovarian metastases, while exhausted $CD8^+$ T cells and Tregs were enriched in peritoneal metastases. These cells not only support immune escape directly but also promote tumor invasion via various non-immunological activities,[65] likely contributes to the establishment of an immunosuppressive microenvironment. More intriguingly, a 30-gene signature of ovarian-derived TAMs was discovered and validated to predict ovarian metastasis in GC. Although evidence has shown that TAMs closely related to most solid tumors, such as ovarian cancer,[66–68] this study was the first time to use the gene signature of ovarian-derived TAM subcluster to forecast ovarian metastasis in GC. Among the top 30 upregulated DEGs of ovarian-derived TAMs, *SPP1*, *IGF1*, *STARD13*, *A2M*, *LPL*, *ASRGL1*, *FABP5*, *SELENOP*, *FOLR2*, *HGF*, *GPR34*, and *BNC2* have been previously confirmed to be highly expressed in ovarian cancer,[69–80] promoting tumorigenesis and metastasis of ovarian cancer cells in GC. Thus, these data further support our findings and highlight the clinical value of the 30-gene signature in TAMs derived from

Figure 5. Key TFs regulating the TGPRNs of PT and M

(A) The TGPRNs of PT, Li, O, LN, and P. Rhombuses represent cell-specific TFs in the same color as the corresponding cell. Circles represent TF-regulated genes that are marker genes in each of the five cancer samples. Rectangles represent the top 10 KEGG pathways where the TF-regulated genes are enriched, with the color intensity representing the magnitude of the *p* value, where darker colors indicate smaller *p* values.

(B) Overall survival curves of the patients with GC in TCGA, stratified by the TF expression levels of the *RUNX2*, *ZNF143*, *CLOCK*, *GABPB1*, *SOX5*, and *KDM5B* genes. The red line shows the survival curve of the patients exhibiting high TF expression levels in the tumor samples (for the top 50% of all samples); the blue line shows the survival curve of the remaining patients (p value < 0.005).

the ovarian metastasis samples to diagnose and prognose ovarian metastasis of GC.

The roles of immune and stromal cells in the TME are now increasingly recognized.[81] In this study, we conducted a comprehensive analysis of the cell developmental trajectories in immune and stromal cell subsets within the TME of both primary and metastatic GC. Compared to other single-cell studies of GC,[6,13] our findings reveal distinct characteristics in the cell developmental trajectories during PT-to-M progression. Intriguingly, in P, we observed that exhausted $CD8^+$ T cells and Tregs were enriched at the early stages of the differentiation trajectory of T cell subsets, while TAMs were predominantly enriched at the early stages of the differentiation trajectory of myeloid cell subsets in O. This particular phenomenon suggests that the establishment of an immunosuppressive environment may drive immune evasion by skewing T and myeloid cell differentiation. We further examined the expression dynamics of DEGs across each cell subsets along the pseudotime axis. This may advance our understanding of TME heterogeneity and dynamics and reveal a subtle connection between immunosuppression and cell differentiation, and with further research, may facilitate potential therapeutic exploitations.

Cell interactions are critical for facilitating information exchange between different cell types, serving as a fundamental mechanism in various biological processes.[82] Therefore, a comprehensive understanding of the cell interactions between primary and metastatic GC is crucial for unraveling the heterogeneity during PT-to-M progression. In this study, a heterogeneous cellular milieu characterized by active crosstalk between stromal cells and other cell clusters was also highlighted, consistent with findings reported in previous studies.[8,83] Endothelial cells can receive the potential immunoregulation factor, *LGALS9*, from macrophages via *MET*, may promote proliferation and invasion of the GC cell line during liver metastasis.[36] Additionally, Tregs can receive the cell adhesion signals, *PVR*, from macrophage via *TIGIT*, may represent a promising target for combined immunotherapy in GC lymph node metastasis.[84] More importantly, the *NECTIN2-TIGIT* axis has been confirmed as a target for immunotherapy in neuroblastoma.[85] Our results revealed that *NECTIN2-TIGIT* mediated the crosstalk between endothelial cells and Tregs, suggesting its potential as a therapeutic target for GC ovarian metastasis. These findings provide important insights into the molecular mechanisms during tumor metastasis and offer valuable guidance for the development of future research directions and therapeutic strategies aimed at targeting these factors.

With their binding-specific DNA sequences, TFs play pivotal roles in various biological processes, including tumorigenesis, migration, and invasion, by regulating downstream genes.[86] There is mounting evidence demonstrating the significant regulatory functions of specific TFs in the genesis, progression, and metastasis of GC.[87] In this study, we constructed seven cell-specific TGPRNs for both primary and metastatic GC and analyzed their heterogeneity by identifying key TFs and elucidating their transcriptional regulatory roles. *RUNX2*, a member of the Runt-related TF family, was identified in the TGPRNs of PT, and it has been previously shown to upregulate extracellular matrix-cell interactions, activate the PI3K-Akt signaling pathway, and promote cell-to-cell adhesion by modulating the target gene *COL1A2*.[88] In the TGPRNs of M, the target gene *COL14A1*, regulated by the TF *SOX5*, was enriched in the process of protein digestion and absorption. The regulation of *COL14A1* by *SOX5* might facilitate the breakdown and uptake of proteins, thereby providing essential energy and materials for cancer cell migration, potentially supporting the metastasis of GC. Of note, we identified a key TF, *CLOCK*, in the TGPRNs of LN, which appeared to play a critical role in facilitating the mutual attraction and migration of tumor and immune cells.[89] This interaction may contribute to lymph node metastasis and is associated with poor survival outcomes in gastric cancer. These key TFs identified in the TGPRNs were not only associated with a poor prognosis but also might promote PT-to-M progression, providing potential targets for therapeutic intervention in GC treatment. Taken together, our observations represent the first attempt to reveal the transcriptional heterogeneity of primary and metastatic GC by constructing the TGPRNs, suggesting the link between key cell-specific TFs and GC progression.

In conclusion, we constructed a comprehensive single-cell transcriptional atlas of primary and metastatic GC, deciphering the multi-dimensional heterogeneities of cellular compositions, developmental trajectories, cell interactions, and transcriptional regulation during PT-to-M progression. Our findings not only identify promising therapeutic targets but also provide a solid foundation for the development of more effective treatment strategies, with the potential to significantly improve patient outcomes in GC.

Limitations of the study

Some limitations need to be acknowledged in this study. First, due to the use of public datasets in our study, this may limit the generalizability of our research findings. Nevertheless, our study offers valuable insights into cellular compositions, developmental trajectories, cell interactions, and transcriptional regulation during the progression from primary to metastatic GC. Second, we acknowledge that the sample sizes in this study might limit the generalizability of our conclusions to all metastatic gastric cancers. Although our findings were validated in independent bulk RNA-seq and scRNA-seq cohort, subsequent scRNA-seq investigations involving paired samples could potentially offer greater insights into the heterogeneity between primary and metastatic GC. Third, although this study characterized the dynamic heterogeneity of primary and metastatic gastric cancer from multiple perspectives, further validation is needed in future studies, especially for comparative analysis from other perspectives.

RESOURCE AVAILABILITY

Lead contact

Requests for further information and resources should be directed to and will be fulfilled by the lead contact, Yunpeng Zhang (zhangyp@hrbmu.edu.cn).

Materials availability

This study did not generate new unique reagents.

Data and code availability

- Data: All data reported in this paper can be accessed from the Gene Expression Omnibus (GEO: https://ncbi.nlm.nih.gov/geo/) and The Cancer Genome Atlas Program (TCGA, GDC: https://portal.gdc.cancer.gov/). This paper analyzes existing, publicly available data. These accession numbers for the datasets are listed in the key resources table.
- Code: This paper does not report original code.
- All other requests: Any additional information required to reanalyze the data reported in this paper is available from the lead contact upon request.

ACKNOWLEDGMENTS

This work was supported by STI2030-Major Projects (2021ZD0202400); National Natural Science Foundation of China (62472131, 62172131, and U23A20166); Heilongjiang Touyan Innovation Team Program; China Postdoctoral Science Foundation (2024M760709).

AUTHOR CONTRIBUTIONS

Y.Z., X.L., and J.B. conceived the study; Y.Z., X.L., and C.H. supervised the study; Y.Z., K.Y., and J.B. contributed to the data curation; Y.Z., K.Y., and C.H. performed the formal analysis; Y.Z., X.L., and C.H. contributed to the funding acquisition; Y.Z., K.Y., and C.H. contributed to the investigation; Y.Z., K.Y., J.C., Q.O., and W.Z. contributed to the methodology and visualization; Y.Z. contributed to the resources; K.Y. and C.H. contributed to the software; J.C., Q.O., and W.Z. contributed to the validation; Y.Z., X.L., and C.H. contributed to the revision of the article; Y.Z. and K.Y. wrote the article with the help of all other authors. All authors edited and proofread the article.

DECLARATION OF INTERESTS

The authors declare no competing interests.

STAR★METHODS

Detailed methods are provided in the online version of this paper and include the following:

- KEY RESOURCES TABLE
- EXPERIMENTAL MODEL AND STUDY PARTICIPANT DETAILS
  - Study design and patients
  - Data collection
  - Public cohorts for bulk transcriptomics
- METHOD DETAILS
  - Data download
  - Quality control, cluster annotation, and data integration
  - Inference of developmental trajectory
  - Cell interaction analysis
  - Regulon activity analysis
  - Survival analysis
  - KEGG enrichment analysis
  - GO enrichment analysis
- QUANTIFICATION AND STATISTICAL ANALYSIS

SUPPLEMENTAL INFORMATION

Supplemental information can be found online at https://doi.org/10.1016/j.isci.2025.111843.

Received: July 1, 2024
Revised: December 12, 2024
Accepted: December 18, 2024
Published: January 20, 2025

REFERENCES

1. Sung, H., Ferlay, J., Siegel, R.L., Laversanne, M., Soerjomataram, I., Jemal, A., and Bray, F. (2021). Global Cancer Statistics 2020: GLOBOCAN Estimates of Incidence and Mortality Worldwide for 36 Cancers in 185 Countries. CA. Cancer J. Clin. *71*, 209–249. https://doi.org/10.3322/caac.21660.
2. Aurello, P., D'Angelo, F., Rossi, S., Bellagamba, R., Cicchini, C., Nigri, G., Ercolani, G., De Angelis, R., and Ramacciato, G. (2007). Classification of lymph node metastases from gastric cancer: comparison between N-site and N-number systems. Our experience and review of the literature. Am. Surg. *73*, 359–366.
3. Li, D., Wang, Y., Dong, C., Chen, T., Dong, A., Ren, J., Li, W., Shu, G., Yang, J., Shen, W., et al. (2023). CST1 inhibits ferroptosis and promotes gastric cancer metastasis by regulating GPX4 protein stability via OTUB1. Oncogene *42*, 83–98. https://doi.org/10.1038/s41388-022-02537-x.
4. Riihimaki, M., Hemminki, A., Sundquist, K., Sundquist, J., and Hemminki, K. (2016). Metastatic spread in patients with gastric cancer. Oncotarget *7*, 52307–52316. https://doi.org/10.18632/oncotarget.10740.
5. Gao, Y., Bado, I., Wang, H., Zhang, W., Rosen, J.M., and Zhang, X.H.F. (2019). Metastasis Organotropism: Redefining the Congenial Soil. Dev. Cell *49*, 375–391. https://doi.org/10.1016/j.devcel.2019.04.012.
6. Deng, G., Zhang, X., Chen, Y., Liang, S., Liu, S., Yu, Z., and Lü, M. (2023). Single-cell transcriptome sequencing reveals heterogeneity of gastric cancer: progress and prospects. Front. Oncol. *13*, 1074268. https://doi.org/10.3389/fonc.2023.1074268.
7. Xie, J.W., Huang, X.B., Chen, Q.Y., Ma, Y.B., Zhao, Y.J., Liu, L.C., Wang, J.B., Lin, J.X., Lu, J., Cao, L.L., et al. (2020). m(6)A modification-mediated BATF2 acts as a tumor suppressor in gastric cancer through inhibition of ERK signaling. Mol. Cancer *19*, 114. https://doi.org/10.1186/s12943-020-01223-4.
8. Jiang, H., Yu, D., Yang, P., Guo, R., Kong, M., Gao, Y., Yu, X., Lu, X., and Fan, X. (2022). Revealing the transcriptional heterogeneity of organ-specific metastasis in human gastric cancer using single-cell RNA Sequencing. Clin. Transl. Med. *12*, e730. https://doi.org/10.1002/ctm2.730.
9. Zhang, P., Yang, M., Zhang, Y., Xiao, S., Lai, X., Tan, A., Du, S., and Li, S. (2019). Dissecting the Single-Cell Transcriptome Network Underlying Gastric Premalignant Lesions and Early Gastric Cancer. Cell Rep. *27*, 1934–1947.e5. https://doi.org/10.1016/j.celrep.2019.04.052.
10. Joung, J., Ma, S., Tay, T., Geiger-Schuller, K.R., Kirchgatterer, P.C., Verdine, V.K., Guo, B., Arias-Garcia, M.A., Allen, W.E., Singh, A., et al. (2023). A transcription factor atlas of directed differentiation. Cell *186*, 209–229.e26. https://doi.org/10.1016/j.cell.2022.11.026.
11. Sathe, A., Grimes, S.M., Lau, B.T., Chen, J., Suarez, C., Huang, R.J., Poultsides, G., and Ji, H.P. (2020). Single-Cell Genomic Characterization Reveals the Cellular Reprogramming of the Gastric Tumor Microenvironment. Clin. Cancer Res. *26*, 2640–2653. https://doi.org/10.1158/1078-0432.CCR-19-3231.
12. Peng, C., Ouyang, Y., Lu, N., and Li, N. (2020). The NF-kappaB Signaling Pathway, the Microbiota, and Gastrointestinal Tumorigenesis: Recent Advances. Front. Immunol. *11*, 1387. https://doi.org/10.3389/fimmu.2020.01387.
13. Cheng, X., Dai, E., Wu, J., Flores, N.M., Chu, Y., Wang, R., Dang, M., Xu, Z., Han, G., Liu, Y., et al. (2024). Atlas of Metastatic Gastric Cancer Links Ferroptosis to Disease Progression and Immunotherapy Response. Gastroenterology *167*, 1345–1357. https://doi.org/10.1053/j.gastro.2024.07.038.
14. Huang, R., Chen, H., Liang, J., Li, Y., Yang, J., Luo, C., Tang, Y., Ding, Y., Liu, X., Yuan, Q., et al. (2021). Dual Role of Reactive Oxygen Species and their Application in Cancer Therapy. J. Cancer *12*, 5543–5561. https://doi.org/10.7150/jca.54699.

15. Wang, R., Song, S., Qin, J., Yoshimura, K., Peng, F., Chu, Y., Li, Y., Fan, Y., Jin, J., Dang, M., et al. (2023). Evolution of immune and stromal cell states and ecotypes during gastric adenocarcinoma progression. Cancer Cell *41*, 1407–1426.e9. https://doi.org/10.1016/j.ccell.2023.06.005.

16. Cheng, S., Li, Z., Gao, R., Xing, B., Gao, Y., Yang, Y., Qin, S., Zhang, L., Ouyang, H., Du, P., et al. (2021). A pan-cancer single-cell transcriptional atlas of tumor infiltrating myeloid cells. Cell *184*, 792–809.e23. https://doi.org/10.1016/j.cell.2021.01.010.

17. Saito, H., Kono, Y., Murakami, Y., Shishido, Y., Kuroda, H., Matsunaga, T., Fukumoto, Y., Osaki, T., Ashida, K., and Fujiwara, Y. (2018). Highly Activated PD-1/PD-L1 Pathway in Gastric Cancer with PD-L1 Expression. Anticancer Res. *38*, 107–112. https://doi.org/10.21873/anticanres.12197.

18. Lv, Y., Zhao, Y., Wang, X., Chen, N., Mao, F., Teng, Y., Wang, T., Peng, L., Zhang, J., Cheng, P., et al. (2019). Increased intratumoral mast cells foster immune suppression and gastric cancer progression through TNF-alpha-PD-L1 pathway. J. Immunother. Cancer *7*, 54. https://doi.org/10.1186/s40425-019-0530-3.

19. Xia, L., Oyang, L., Lin, J., Tan, S., Han, Y., Wu, N., Yi, P., Tang, L., Pan, Q., Rao, S., et al. (2021). The cancer metabolic reprogramming and immune response. Mol. Cancer *20*, 28. https://doi.org/10.1186/s12943-021-01316-8.

20. Lafront, C., Germain, L., Campolina-Silva, G.H., Weidmann, C., Berthiaume, L., Hovington, H., Brisson, H., Jobin, C., Frégeau-Proulx, L., Cotau, R., et al. (2024). The estrogen signaling pathway reprograms prostate cancer cell metabolism and supports proliferation and disease progression. J. Clin. Invest. *134*, e170809. https://doi.org/10.1172/JCI170809.

21. Peng, P., Liu, X., Yang, L., Gu, Z., and Cai, L. (2023). Systematically Prognostic Analyses of Gastric Cancer Patients with Ovarian Metastasis. Genet. Res. *2023*, 9923428. https://doi.org/10.1155/2023/9923428.

22. Mirzaei, S., Saghari, S., Bassiri, F., Raesi, R., Zarrabi, A., Hushmandi, K., Sethi, G., and Tergaonkar, V. (2022). NF-kappaB as a regulator of cancer metastasis and therapy response: A focus on epithelial-mesenchymal transition. J. Cell. Physiol. *237*, 2770–2795. https://doi.org/10.1002/jcp.30759.

23. Gonda, T.J., and Ramsay, R.G. (2015). Directly targeting transcriptional dysregulation in cancer. Nat. Rev. Cancer *15*, 686–694. https://doi.org/10.1038/nrc4018.

24. Zheng, H.C., Xue, H., Zhang, C.Y., Shi, K.H., and Zhang, R. (2022). The roles of BTG1 mRNA expression in cancers: A bioinformatics analysis. Front. Genet. *13*, 1006636. https://doi.org/10.3389/fgene.2022.1006636.

25. Guo, F., Ren, X., Dong, Y., Hu, X., Xu, D., Zhou, H., Meng, F., Tian, W., and Zhao, Y. (2016). Constitutive expression of PPARgamma inhibits proliferation and migration of gastric cancer cells and down-regulates Wnt/beta-Catenin signaling pathway downstream target genes TERT and ENAH. Gene *584*, 31–37. https://doi.org/10.1016/j.gene.2016.03.003.

26. Jiang, T., Xia, Y., Lv, J., Li, B., Li, Y., Wang, S., Xuan, Z., Xie, L., Qiu, S., He, Z., et al. (2021). A novel protein encoded by circMAPK1 inhibits progression of gastric cancer by suppressing activation of MAPK signaling. Mol. Cancer *20*, 66. https://doi.org/10.1186/s12943-021-01358-y.

27. Quintanal-Villalonga, Á., Chan, J.M., Yu, H.A., Pe'er, D., Sawyers, C.L., Sen, T., and Rudin, C.M. (2020). Lineage plasticity in cancer: a shared pathway of therapeutic resistance. Nat. Rev. Clin. Oncol. *17*, 360–371. https://doi.org/10.1038/s41571-020-0340-z.

28. Harjunpaa, H., Llort Asens, M., Guenther, C., and Fagerholm, S.C. (2019). Cell Adhesion Molecules and Their Roles and Regulation in the Immune and Tumor Microenvironment. Front. Immunol. *10*, 1078. https://doi.org/10.3389/fimmu.2019.01078.

29. Li, Y., Mo, N., Yang, D., Lin, Q., Huang, W., and Wang, R. (2023). Predictive value of DNA methylation in the efficacy of chemotherapy for gastric cancer. Front. Oncol. *13*, 1238310. https://doi.org/10.3389/fonc.2023.1238310.

30. Rong, L., Li, Z., Leng, X., Li, H., Ma, Y., Chen, Y., and Song, F. (2020). Salidroside induces apoptosis and protective autophagy in human gastric cancer AGS cells through the PI3K/Akt/mTOR pathway. Biomed. Pharmacother. *122*, 109726. https://doi.org/10.1016/j.biopha.2019.109726.

31. Zhang, L.Q., Zhou, S.L., Li, J.K., Chen, P.N., Zhao, X.K., Wang, L.D., Li, X.L., and Zhou, F.Y. (2022). Identification of a seven-cell cycle signature predicting overall survival for gastric cancer. Aging (Albany NY) *14*, 3989–3999. https://doi.org/10.18632/aging.204060.

32. Wang, Y., Zheng, L., Shang, W., Yang, Z., Li, T., Liu, F., Shao, W., Lv, L., Chai, L., Qu, L., et al. (2022). Wnt/beta-catenin signaling confers ferroptosis resistance by targeting GPX4 in gastric cancer. Cell Death Differ. *29*, 2190–2202. https://doi.org/10.1038/s41418-022-01008-w.

33. Zeng, C., He, R., Dai, Y., Lu, X., Deng, L., Zhu, Q., Liu, Y., Liu, Q., Lu, W., Wang, Y., and Jin, J. (2022). Identification of TGF-beta signaling-related molecular patterns, construction of a prognostic model, and prediction of immunotherapy response in gastric cancer. Front. Pharmacol. *13*, 1069204. https://doi.org/10.3389/fphar.2022.1069204.

34. Ohue, Y., and Nishikawa, H. (2019). Regulatory T (Treg) cells in cancer: Can Treg cells be a new therapeutic target? Cancer Sci. *110*, 2080–2089. https://doi.org/10.1111/cas.14069.

35. Du, X., Cheng, Z., Wang, Y.H., Guo, Z.H., Zhang, S.Q., Hu, J.K., and Zhou, Z.G. (2014). Role of Notch signaling pathway in gastric cancer: a meta-analysis of the literature. World J. Gastroenterol. *20*, 9191–9199. https://doi.org/10.3748/wjg.v20.i27.9191.

36. Yang, K., Yang, T., Yu, J., Li, F., and Zhao, X. (2023). Integrated transcriptional analysis reveals macrophage heterogeneity and macrophage-tumor cell interactions in the progression of pancreatic ductal adenocarcinoma. BMC Cancer *23*, 199. https://doi.org/10.1186/s12885-023-10675-y.

37. Seidlitz, T., Schmäche, T., García, F., Lee, J.H., Qin, N., Kochall, S., Fohgrub, J., Pauck, D., Rothe, A., Koo, B.K., et al. (2022). Sensitivity towards HDAC inhibition is associated with RTK/MAPK pathway activation in gastric cancer. EMBO Mol. Med. *14*, e15705. https://doi.org/10.15252/emmm.202215705.

38. Ho, D.W.H., Tsui, Y.M., Chan, L.K., Sze, K.M.F., Zhang, X., Cheu, J.W.S., Chiu, Y.T., Lee, J.M.F., Chan, A.C.Y., Cheung, E.T.Y., et al. (2021). Single-cell RNA sequencing shows the immunosuppressive landscape and tumor heterogeneity of HBV-associated hepatocellular carcinoma. Nat. Commun. *12*, 3684. https://doi.org/10.1038/s41467-021-24010-1.

39. Li, M., Liu, G., Jin, X., Guo, H., Setrerrahmane, S., Xu, X., Li, T., Lin, Y., and Xu, H. (2022). Micropeptide MIAC inhibits the tumor progression by interacting with AQP2 and inhibiting EREG/EGFR signaling in renal cell carcinoma. Mol. Cancer *21*, 181. https://doi.org/10.1186/s12943-022-01654-1.

40. Gorvel, L., and Olive, D. (2020). Targeting the "PVR-TIGIT axis" with immune checkpoint therapies. F1000Res. *9*, F1000FacultyRev-354. https://doi.org/10.12688/f1000research.22877.1.

41. Lee, B.S., Jang, J.Y., Seo, C., and Kim, C.H. (2021). Crosstalk between head and neck cancer cells and lymphatic endothelial cells promotes tumor metastasis via CXCL5-CXCR2 signaling. FASEB J. *35*, e21181. https://doi.org/10.1096/fj.202001455R.

42. Bu, J., Yan, W., Huang, Y., and Lin, K. (2023). Activation of the IL-17 signalling pathway by the CXCL17-GPR35 axis affects drug resistance and colorectal cancer tumorigenesis. Am. J. Cancer Res. *13*, 2172–2187.

43. Arnal-Estape, A., Cai, W.L., Albert, A.E., Zhao, M., Stevens, L.E., Lopez-Giraldez, F., Patel, K.D., Tyagi, S., Schmitt, E.M., Westbrook, T.F., and Nguyen, D.X. (2020). Tumor progression and chromatin landscape of lung cancer are regulated by the lineage factor GATA6. Oncogene *39*, 3726–3737. https://doi.org/10.1038/s41388-020-1246-z.

44. Li, Y., Sun, R., Zhao, X., and Sun, B. (2021). RUNX2 promotes malignant progression in gastric cancer by regulating COL1A1. Cancer Biomark. *31*, 227–238. https://doi.org/10.3233/CBM-200472.

45. Xu, X., Liu, Z., Tian, F., Xu, J., and Chen, Y. (2019). Clinical Significance of Transcription Factor 7 (TCF7) as a Prognostic Factor in Gastric Cancer. Med. Sci. Monit. *25*, 3957–3963. https://doi.org/10.12659/MSM.913913.

46. Cui, J., Xi, H., Cai, A., Bian, S., Wei, B., and Chen, L. (2014). Decreased expression of Sox7 correlates with the upregulation of the Wnt/beta-catenin signaling pathway and the poor survival of gastric cancer patients. Int. J. Mol. Med. *34*, 197–204. https://doi.org/10.3892/ijmm.2014.1759.

47. Zhang, Y., Wang, B., Song, H., and Han, M. (2023). GLIS3, a novel prognostic indicator of gastric adenocarcinoma, contributes to the malignant biological behaviors of tumor cells via modulating TGF-beta1/TGFbetaR1/Smad1/5 signaling pathway. Cytokine *170*, 156342. https://doi.org/10.1016/j.cyto.2023.156342.

48. Chen, J.J., Ren, Y.L., Shu, C.J., Zhang, Y., Chen, M.J., Xu, J., Li, J., Li, A.P., Chen, D.Y., He, J.D., et al. (2020). JP3, an antiangiogenic peptide, inhibits growth and metastasis of gastric cancer through TRIM25/SP1/MMP2 axis. J. Exp. Clin. Cancer Res. *39*, 118. https://doi.org/10.1186/s13046-020-01617-8.

49. Zhang, B., Wu, J., Cai, Y., Luo, M., Wang, B., and Gu, Y. (2019). TCF7L1 indicates prognosis and promotes proliferation through activation of Keap1/NRF2 in gastric cancer. Acta Biochim. Biophys. Sin. *51*, 375–385. https://doi.org/10.1093/abbs/gmz015.

50. Li, X., Xie, G., Chen, J., Wang, Y., Zhai, J., and Shen, L. (2024). Tumour cell-derived serglycin promotes IL-8 secretion of CAFs in gastric cancer. Br. J. Cancer *131*, 271–282. https://doi.org/10.1038/s41416-024-02735-2.

51. Cao, L., Wang, S., Zhang, Y., Wong, K.C., Nakatsu, G., Wang, X., Wong, S., Ji, J., and Yu, J. (2018). Zinc-finger protein 471 suppresses gastric cancer through transcriptionally repressing downstream oncogenic PLS3 and TFAP2A. Oncogene *37*, 3601–3616. https://doi.org/10.1038/s41388-018-0220-5.

52. Panni, S., Lovering, R.C., Porras, P., and Orchard, S. (2020). Non-coding RNA regulatory networks. Biochim. Biophys. Acta. Gene Regul. Mech. *1863*, 194417. https://doi.org/10.1016/j.bbagrm.2019.194417.

53. Zhang, P., Cao, X., Guan, M., Li, D., Xiang, H., Peng, Q., Zhou, Y., Weng, C., Fang, X., Liu, X., et al. (2022). CPNE8 Promotes Gastric Cancer Metastasis by Modulating Focal Adhesion Pathway and Tumor Microenvironment. Int. J. Biol. Sci. *18*, 4932–4949. https://doi.org/10.7150/ijbs.76425.

54. Tsoi, L.C., Spain, S.L., Knight, J., Ellinghaus, E., Stuart, P.E., Capon, F., Ding, J., Li, Y., Tejasvi, T., Gudjonsson, J.E., et al. (2012). Identification of 15 new psoriasis susceptibility loci highlights the role of innate immunity. Nat. Genet. *44*, 1341–1348. https://doi.org/10.1038/ng.2467.

55. Gray, G.M., and Cooper, H.L. (1971). Protein digestion and absorption. Gastroenterology *61*, 535–544.

56. Moradi-Marjaneh, R., Hassanian, S.M., Fiuji, H., Soleimanpour, S., Ferns, G.A., Avan, A., and Khazaei, M. (2018). Toll like receptor signaling pathway as a potential therapeutic target in colorectal cancer. J. Cell. Physiol. *233*, 5613–5622. https://doi.org/10.1002/jcp.26273.

57. Jiang, Z., Lim, S.O., Yan, M., Hsu, J.L., Yao, J., Wei, Y., Chang, S.S., Yamaguchi, H., Lee, H.H., Ke, B., et al. (2021). TYRO3 induces anti-PD-1/PD-L1 therapy resistance by limiting innate immunity and tumoral ferroptosis. J. Clin. Invest. *131*, e139434. https://doi.org/10.1172/JCI139434.

58. Dermani, F.K., Samadi, P., Rahmani, G., Kohlan, A.K., and Najafi, R. (2019). PD-1/PD-L1 immune checkpoint: Potential target for cancer therapy. J. Cell. Physiol. *234*, 1313–1325. https://doi.org/10.1002/jcp.27172.

59. Chen, K., Wang, Y., Hou, Y., Wang, Q., Long, D., Liu, X., Tian, X., and Yang, Y. (2022). Single cell RNA-seq reveals the CCL5/SDC1 receptor-ligand interaction between T cells and tumor cells in pancreatic cancer. Cancer Lett. *545*, 215834. https://doi.org/10.1016/j.canlet.2022.215834.

60. DeCordova, S., Shastri, A., Tsolaki, A.G., Yasmin, H., Klein, L., Singh, S.K., and Kishore, U. (2020). Molecular Heterogeneity and Immunosuppressive Microenvironment in Glioblastoma. Front. Immunol. *11*, 1402. https://doi.org/10.3389/fimmu.2020.01402.

61. S, N.K., Wilson, G.W., Grant, R.C., Seto, M., O'Kane, G., Vajpeyi, R., Notta, F., Gallinger, S., and Chetty, R. (2020). Morphological classification of pancreatic ductal adenocarcinoma that predicts molecular subtypes and correlates with clinical outcome. Gut *69*, 317–328. https://doi.org/10.1136/gutjnl-2019-318217.

62. Li, P.H., Kong, X.Y., He, Y.Z., Liu, Y., Peng, X., Li, Z.H., Xu, H., Luo, H., and Park, J. (2022). Recent developments in application of single-cell RNA sequencing in the tumour immune microenvironment and cancer therapy. Mil. Med. Res. *9*, 52. https://doi.org/10.1186/s40779-022-00414-y.

63. Tran, H.T.N., Ang, K.S., Chevrier, M., Zhang, X., Lee, N.Y.S., Goh, M., and Chen, J. (2020). A benchmark of batch-effect correction methods for single-cell RNA sequencing data. Genome Biol. *21*, 12. https://doi.org/10.1186/s13059-019-1850-9.

64. Kim, N., Kim, H.K., Lee, K., Hong, Y., Cho, J.H., Choi, J.W., Lee, J.I., Suh, Y.L., Ku, B.M., Eum, H.H., et al. (2020). Single-cell RNA sequencing demonstrates the molecular and cellular reprogramming of metastatic lung adenocarcinoma. Nat. Commun. *11*, 2285. https://doi.org/10.1038/s41467-020-16164-1.

65. Li, K., Shi, H., Zhang, B., Ou, X., Ma, Q., Chen, Y., Shu, P., Li, D., and Wang, Y. (2021). Myeloid-derived suppressor cells as immunosuppressive regulators and therapeutic targets in cancer. Signal Transduct. Target. Ther. *6*, 362. https://doi.org/10.1038/s41392-021-00670-9.

66. Puttock, E.H., Tyler, E.J., Manni, M., Maniati, E., Butterworth, C., Burger Ramos, M., Peerani, E., Hirani, P., Gauthier, V., Liu, Y., et al. (2023). Extracellular matrix educates an immunoregulatory tumor macrophage phenotype found in ovarian cancer metastasis. Nat. Commun. *14*, 2514. https://doi.org/10.1038/s41467-023-38093-5.

67. Wang, H., Yung, M.M.H., Ngan, H.Y.S., Chan, K.K.L., and Chan, D.W. (2021). The Impact of the Tumor Microenvironment on Macrophage Polarization in Cancer Metastatic Progression. Int. J. Mol. Sci. *22*, 6560. https://doi.org/10.3390/ijms22126560.

68. Yousefi, M., Dehghani, S., Nosrati, R., Ghanei, M., Salmaninejad, A., Rajaie, S., Hasanzadeh, M., and Pasdar, A. (2020). Current insights into the metastasis of epithelial ovarian cancer - hopes and hurdles. Cell. Oncol. *43*, 515–538. https://doi.org/10.1007/s13402-020-00513-9.

69. Cesaratto, L., Grisard, E., Coan, M., Zandonà, L., De Mattia, E., Poletto, E., Cecchin, E., Puglisi, F., Canzonieri, V., Mucignat, M.T., et al. (2016). BNC2 is a putative tumor suppressor gene in high-grade serous ovarian carcinoma and impacts cell survival after oxidative stress. Cell Death Dis. *7*, e2374. https://doi.org/10.1038/cddis.2016.278.

70. Xu, Y., Tan, S., Huang, W., and Wang, Y.X. (2023). Construction of monocyte-related prognosis model based on comprehensive analysis of bulk RNA-seq and single-cell RNA-seq in high-grade serous ovarian cancer. Medicine (Baltim.) *102*, e36548. https://doi.org/10.1097/MD.0000000000036548.

71. Liu, J., Li, J., Wu, X., Zhang, M., Yan, G., Sun, H., and Li, D. (2024). High levels of fatty acid-binding protein 5 excessively enhances fatty acid synthesis and proliferation of granulosa cells in polycystic ovary syndrome. J. Ovarian Res. *17*, 44. https://doi.org/10.1186/s13048-024-01368-6.

72. Ma, S., Li, R., Li, G., Wei, M., Li, B., Li, Y., and Ha, C. (2024). Identification of a G-protein coupled receptor-related gene signature through bioinformatics analysis to construct a risk model for ovarian cancer prognosis. Comput. Biol. Med. *178*, 108747. https://doi.org/10.1016/j.compbiomed.2024.108747.

73. Sutphen, R., Xu, Y., Wilbanks, G.D., Fiorica, J., Grendys, E.C., Jr., LaPolla, J.P., Arango, H., Hoffman, M.S., Martino, M., Wakeley, K., et al. (2004). Lysophospholipids are potential biomarkers of ovarian cancer. Cancer Epidemiol. Biomarkers Prev. *13*, 1185–1191.

74. Wang, K., Hou, H., Zhang, Y., Ao, M., Luo, H., and Li, B. (2023). Ovarian cancer-associated immune exhaustion involves SPP1+ T cell and NKT cell, symbolizing more malignant progression. Front. Endocrinol. *14*, 1168245. https://doi.org/10.3389/fendo.2023.1168245.

75. Lv, X.F., Hong, H.Q., Liu, L., Cui, S.H., Ren, C.C., Li, H.Y., Zhang, X.A., Zhang, L.D., Wei, T.X., Liu, J.J., et al. (2018). RNAi-mediated downregulation of asparaginase-like protein 1 inhibits growth and promotes apoptosis of human cervical cancer line SiHa. Mol. Med. Rep. *18*, 931–937. https://doi.org/10.3892/mmr.2018.9018.

76. Qazi, I.H., Angel, C., Yang, H., Pan, B., Zoidis, E., Zeng, C.J., Han, H., and Zhou, G.B. (2018). Selenium, Selenoproteins, and Female Reproduction: A Review. Molecules *23*, 3053. https://doi.org/10.3390/molecules23123053.

77. Abdellatef, S., Fakhoury, I., Haddad, M.A., Jaafar, L., Maalouf, H., Hanna, S., Khalil, B., El Masri, Z., Hodgson, L., and El-Sibai, M. (2022). StarD13 negatively regulates invadopodia formation and invasion in high-grade serous (HGS) ovarian adenocarcinoma cells by inhibiting Cdc42. Eur. J. Cell Biol. *101*, 151197. https://doi.org/10.1016/j.ejcb.2021.151197.

78. Penn, C.A., Yang, K., Zong, H., Lim, J.Y., Cole, A., Yang, D., Baker, J., Goonewardena, S.N., and Buckanovich, R.J. (2018). Therapeutic Impact of Nanoparticle Therapy Targeting Tumor-Associated Macrophages. Mol. Cancer Ther. *17*, 96–106. https://doi.org/10.1158/1535-7163.MCT-17-0688.

79. Kim, H.J. (2022). Therapeutic Strategies for Ovarian Cancer in Point of HGF/c-MET Targeting. Medicina (Kaunas) *58*, 649. https://doi.org/10.3390/medicina58050649.

80. Li, Y., Wang, F., Liu, T., Lv, N., Yuan, X., and Li, P. (2022). WISP1 induces ovarian cancer via the IGF1/alphavbeta3/Wnt axis. J. Ovarian Res. *15*, 94. https://doi.org/10.1186/s13048-022-01016-x.

81. Kumar, V., Ramnarayanan, K., Sundar, R., Padmanabhan, N., Srivastava, S., Koiwa, M., Yasuda, T., Koh, V., Huang, K.K., Tay, S.T., et al. (2022). Single-Cell Atlas of Lineage States, Tumor Microenvironment, and Subtype-Specific Expression Programs in Gastric Cancer. Cancer Discov. *12*, 670–691. https://doi.org/10.1158/2159-8290.CD-21-0683.

82. Liu, Z., Sun, D., and Wang, C. (2022). Evaluation of cell-cell interaction methods by integrating single-cell RNA sequencing data with spatial information. Genome Biol. *23*, 218. https://doi.org/10.1186/s13059-022-02783-y.

83. Wan, Q., Wei, R., Wei, X., and Deng, Y.P. (2022). Crosstalk of four kinds of cell deaths defines subtypes of cutaneous melanoma for precise immunotherapy and chemotherapy. Front. Immunol. *13*, 998454. https://doi.org/10.3389/fimmu.2022.998454.

84. Zhou, X., Li, Y., Zhang, X., Li, B., Jin, S., Wu, M., Zhou, X., Dong, Q., Du, J., Zhai, W., et al. (2024). Hemin blocks TIGIT/PVR interaction and induces ferroptosis to elicit synergistic effects of cancer immunotherapy. Sci. China Life Sci. *67*, 996–1009. https://doi.org/10.1007/s11427-023-2472-4.

85. Wienke, J., Visser, L.L., Kholosy, W.M., Keller, K.M., Barisa, M., Poon, E., Munnings-Tomes, S., Himsworth, C., Calton, E., Rodriguez, A., et al. (2024). Integrative analysis of neuroblastoma by single-cell RNA sequencing identifies the NECTIN2-TIGIT axis as a target for immunotherapy. Cancer Cell *42*, 283–300.e8. https://doi.org/10.1016/j.ccell.2023.12.008.

86. de Mendoza, A., and Sebé-Pedrós, A. (2019). Origin and evolution of eukaryotic transcription factors. Curr. Opin. Genet. Dev. *58–59*, 25–32. https://doi.org/10.1016/j.gde.2019.07.010.

87. Abadi, A.J., Zarrabi, A., Hashemi, F., Zabolian, A., Najafi, M., Entezari, M., Hushmandi, K., Aref, A.R., Khan, H., Makvandi, P., et al. (2021). The role of SOX family transcription factors in gastric cancer. Int. J. Biol. Macromol. *180*, 608–624. https://doi.org/10.1016/j.ijbiomac.2021.02.202.

88. Wang, Y., Chu, F., Lin, J., Li, Y., Johnson, N., Zhang, J., Gai, C., Su, Z., Cheng, H., Wang, L., and Ding, X. (2021). Erianin, the main active ingredient of Dendrobium chrysotoxum Lindl, inhibits precancerous lesions of gastric cancer (PLGC) through suppression of the HRAS-PI3K-AKT signaling pathway as revealed by network pharmacology and *in vitro* experimental verification. J. Ethnopharmacol. *279*, 114399. https://doi.org/10.1016/j.jep.2021.114399.

89. Pang, L., Dunterman, M., Xuan, W., Gonzalez, A., Lin, Y., Hsu, W.H., Khan, F., Hagan, R.S., Muller, W.A., Heimberger, A.B., and Chen, P. (2023). Circadian regulator CLOCK promotes tumor angiogenesis in glioblastoma. Cell Rep. *42*, 112127. https://doi.org/10.1016/j.celrep.2023.112127.

90. Efremova, M., Vento-Tormo, M., Teichmann, S.A., and Vento-Tormo, R. (2020). CellPhoneDB: inferring cell-cell communication from combined expression of multi-subunit ligand-receptor complexes. Nat. Protoc. *15*, 1484–1506. https://doi.org/10.1038/s41596-020-0292-x.

91. Kumar, N., Mishra, B., Athar, M., and Mukhtar, S. (2021). Inference of Gene Regulatory Network from Single-Cell Transcriptomic Data Using pySCENIC. Methods Mol. Biol. *2328*, 171–182. https://doi.org/10.1007/978-1-0716-1534-8_10.

92. Liao, C., and Wang, X. (2023). TCGAplot: an R package for integrative pancancer analysis and visualization of TCGA multi-omics data. BMC Bioinf. *24*, 483. https://doi.org/10.1186/s12859-023-05615-3.

93. Xu, S., Hu, E., Cai, Y., Xie, Z., Luo, X., Zhan, L., Tang, W., Wang, Q., Liu, B., Wang, R., et al. (2024). Using clusterProfiler to characterize multiomics data. Nat. Protoc. *19*, 3292–3320. https://doi.org/10.1038/s41596-024-01020-z.

STAR★METHODS

KEY RESOURCES TABLE

REAGENT or RESOURCE	SOURCE	IDENTIFIER
Deposited data		
GC scRNA-seq (GSE163558)	Jiang et al., 2022	GEO: https://www.ncbi.nlm.nih.gov/geo/query/acc.cgi
GC scRNA-seq (GSE239676)	Cheng et al., 2024	GEO: https://www.ncbi.nlm.nih.gov/geo/query/acc.cgi
GC bulk RNA-seq (GSE84437)	Yoon et al., 2020	GEO: https://www.ncbi.nlm.nih.gov/geo/query/acc.cgi
GC bulk RNA-seq TCGA-STAD	TCGA via cgdsr	https://www.cancer.gov/ccg/research/genome-sequencing/tcga
Software and algorithms		
R (v4.2.2)	R CRAN	https://cran.r-project.org/
clusterProfiler pipeline	clusterProfiler package in R	v4.0.5
ggplot2 pipeline	ggplot2 package in R	v3.4.4
cgdsr pipeline	cgdsr package in R	v1.3.0
monocle2 pipeline	monocle package in R	v2.26.0
Seurat pipeline	Seurat package in R	v4.3.0.1
pheatmap pipeline	pheatmap package in R	v1.0.12
survminer pipeline	survminer package in R	v0.4.9
survival pipeline	survival package in R	v3.5-8
RColorBrewer pipeline	RColorBrewer package in R	v1.1-3
AUCell pipeline	AUCell package in R	v1.26.0
SCENIC pipeline	SCENIC package in R	v1.3.1
ggvenn pipeline	ggvenn package in R	v0.1.10
circlize pipeline	circlize package in R	v0.4.16
org.Hs.eg.db pipeline	org.Hs.eg.db package in R	v3.19.1
ktplots pipeline	ktplots package in R	v2.4.0
CellChat pipeline	CellChat package in R	v1.6.1
gplots pipeline	gplots package in R	v3.1.3.1
TCGAplot pipeline	TCGAplot package in R	v7.0.1
Python (v3.7.0)	Python Software Foundation	https://www.python.org
CellPhoneDB	cellphonedb in python	v4.0.0
pySCENIC	pySCENIC in python	v0.12.1
Cytoscape	https://cytoscape.org/	v3.9.1

EXPERIMENTAL MODEL AND STUDY PARTICIPANT DETAILS

Study design and patients

The public GEO dataset GSE163558 was used in this study. The dataset includes a total of 54,687 cells derived from 10 fresh human tissue samples from six patients. The clinical information of all patients is summarized in Table S10.

Data collection

Public single cell data were obtained from the GEO database. GSE163558 and GSE239676 provided the output files of the CellRanger (10x Genomics) pipeline.

Public cohorts for bulk transcriptomics

RNA-seq and clinical data from patients with gastric adenocarcinoma (cancer study ID: STAD TCGA) were obtained from TCGA using the R package cgdsr. We also download another large-scale primary GAC dataset (GSE84437) from the GEO database.

METHOD DETAILS

Data download

The single-cell RNA sequencing dataset GSE163558 was obtained from the GEO database (GEO: https://www.ncbi.nlm.nih.gov/gds). This dataset includes a total of 54,687 cells derived from 10 fresh human tissue samples from six patients. The samples consist of primary tumor tissue, adjacent non-tumor tissue, and six metastatic samples from various organs, such as the liver, peritoneum, ovary, and lymph node.

Quality control, cluster annotation, and data integration

For data normalization, dimensionality reduction, and clustering, we employed Seurat v.4.3.0.1 in R v.4.2.2, accessed from https://github.com/satijalab/seurat. The quality of cells was assessed based on total UMI count per cell, total detected genes per cell, and proportion of mitochondrial genes per cell. Low-quality cells were filtered following these criteria: (1) cells with < 200 genes; (2) cells with < 700 UMI count or ranked in the top 1% of UMI counts; (3) cells with > 20% mitochondrial gene count. Genes detected in less than three cells were also excluded from downstream analyses. Subsequently, data integration was performed using the IntegrateData() function. After quality control, a total of 42,968 cells were retained. To identify cluster-specific marker genes, we utilized the Seurat FindMarkers function with default parameters and applied the Wilcoxon rank-sum test for the analysis of DEGs between the specific cluster and all other clusters. Significant DEGs were defined as $|\log2(\text{Fold Change})| > 1$ and p-value < 0.05. In addition, mitochondrial and ribosomal genes were filtered out from the DEG lists. Finally, we performed manual cell annotation based on the expression of these significant cell marker genes for subsequent downstream analyses.

Inference of developmental trajectory

The Monocle2 algorithm was employed to infer potential cell lineage trajectories between diverse cell phenotypes. The UMI count matrix served as the input data. To reduce dimensionality, a CellDataSet object was created using the newCellDataSet function with the expressionFamily = Negbinomial.size() parameter, and the DDRTree algorithm was applied. Cell clusters and pseudotemporal cell trajectories were deduced based on cell clustering and pseudotemporal cell sorting, by utilizing Monocle2's default parameters. The resulting trajectories were visualized using the Plot_cell_Track function. Pseudotime-dependent genes, indicating expression differences over pseudotime, were identified along the cell developmental trajectories through the Differential GeneTest function. The Plot_gene_in_Passotime and Plot_Passotime_heatmap functions were employed to visually represent the dynamic changes in gene expression dependent on pseudotime. The heatmaps were generated to illustrate the top 30 significant genes that exhibited pseudotime-dependent expression during PT-to-M progression.

Cell interaction analysis

CellPhoneDB (version 4.0.0) was used to analyze cell interactions between diverse cell types.[90] In brief, for each gene in each cell type, the average expression value of the gene and the percentage of cells expressing the gene were calculated. Potential receptor-ligand interactions between cell types were inferred based on the expression of receptors in one cell type and ligands in the other. The cell type labels of all cells were then randomly permuted 1000 times to test the statistical significance of the estimated receptor-ligand interaction. The intensity of the receptor-ligand interactions was assessed based on the expression of the ligand-receptor pairs in two cell types.

Regulon activity analysis

The gene regulatory network (GRN) was constructed using the pySCENIC[91] algorithm, in conjunction with the GRNBoost2 algorithm in the Arboreto software package and the cis-Target human motif database (V9) for all cells. Raw expression data and labeled clusters from the Seurat data were utilized and subjected to filtration using the default parameters of the pySCENIC pipeline. Subsequently, the GRNBoost2 method was employed to compute the GRNs. CisTarget databases, including hg19-500bp-upstream-10species.mc9nr.genes_vs_motifs.rankings.feather and hg19-tss-centered-10kb-10species.mc9nr.genes_vs_motifs.rankings.feather, were used to identify the enriched motifs, along with the TF motif annotation database (v9). The Aucell function scored all cells to display the regulon activities. The similarity score for the regulons in each cluster was computed and transferred to the specific score using Jensen-Shannon divergence.

Survival analysis

RNA-seq and clinical data from patients with gastric adenocarcinoma (cancer study ID: STAD TCGA) were obtained from TCGA using the R package cgdsr. Tumor samples were classified into two groups based on the median expression of key TFs between all patients. Survival analysis was performed using the Kaplan-Meier method in the R package Survival. The survival curve was visualized using the ggsurvplot function from the R package survminer. Both survival analysis and visualization were conducted using the R package. In addition, *CLOCK* expression was verified in other cancers using the R package TCGAplot.[92]

KEGG enrichment analysis

To assess gene expression signatures and pathway activation, KEGG analysis was performed using the DEGs of five cancer samples in the TME of primary and metastatic GC. The enrichKEGG function from the clusterProfiler R package was utilized for this analysis.[93] A significance threshold of p-value < .05 was set, and the top 10 most significant pathways were visualized using ggplot2 R package.

GO enrichment analysis

The top 100 upregulated DEGs of each cluster were then used to perform GO analysis using clusterProfiler R package, and the functional gene sets belonging to biological process were focused on this study. The q value was used to select the significantly enriched results with a cutoff value of .05. The results of GO enrichment analysis are filtered according to the q value (qvalueCutoff = .05).

QUANTIFICATION AND STATISTICAL ANALYSIS

The statistical tests used here are indicated in the relevant figure legends. Data are presented as the mean ± standard deviation (SD) or median (interquartile range, IQR). We used the Wilcoxon rank-sum test to assess differences in AUCell scores of the 30-gene signature from ovarian-derived TAMs between non-ovarian metastasis groups. The distribution of *CLOCK* gene expression levels in tumor samples versus normal samples for multiple cancer types was analyzed using the Wilcoxon rank-sum test. To identify marker genes expressed in each subset and the differentially expressed genes between the Student's t-test, we used the Student's t-test implemented in Seurat. Statistical analyses and graph generation were conducted in R (version 4.2.2) and Python (version 3.7.0). A p value of less than 0.05 was considered statistically significant, * $p < 0.05$, ** $p < 0.01$, *** $p < 0.001$, **** $p < 0.0001$.